MIT Libraries | DSpace@MIT

MIT Open Access Articles

Falling film boiling of refrigerants over nanostructured and roughened tubes: Heat transfer, dryout and critical heat flux

The MIT Faculty has made this article openly available. ***Please share*** how this access benefits you. Your story matters.

As Published: 10.1016/j.ijheatmasstransfer.2020.120452

Publisher: Elsevier BV

Persistent URL: https://hdl.handle.net/1721.1/133355

Version: Author's final manuscript: final author's manuscript post peer review, without publisher's formatting or copy editing

Terms of use: Creative Commons Attribution-NonCommercial-NoDerivs License

Massachusetts Institute of Technology

Falling film boiling of refrigerants over nanostructured and roughened tubes: Heat transfer, dryout and critical heat flux

This is the PREPRINT version of this article. The final, published version of the article can be found at: https://doi.org/10.1016/j.ijheatmasstransfer.2020.120452

Bradley D. Bock[a], Matteo Bucci[b], Christos N. Markides[c], John R. Thome[d] and Josua P. Meyer[a,*]

[a]*Department of Mechanical and Aeronautical Engineering, Faculty of Engineering, the Built Environment and IT, University of Pretoria, Pretoria, South Africa*
[b]*Department of Nuclear Science and Engineering, Massachusetts Institute of Technology (MIT), Cambridge, MA, 02139, USA*
[c]*Clean Energy Processes (CEP) Laboratory, Department of Chemical Engineering, Imperial College London, London, SW7 2AZ, UK*
[d]*Institute for Multiscale Thermofluids, School of Engineering, University of Edinburgh, Edinburgh, UK and JJ Cooling Innovation Sàrl, Lausanne, Switzerland*

Abstract

Falling film evaporators offer an attractive alternative to flooded evaporators as the lower fluid charge reduces the impact of leaks to the environment and associated safety concerns. A study was conducted of saturated falling film boiling of two refrigerants on one polished, one roughened and three nanostructured copper tubes in order to evaluate the potential of nanostructures in falling film refrigerant evaporators. Tubes were individually tested, placed horizontally within a test chamber and heated by an internal water flow with refrigerant distributed over the outside of the tubes. Wilson plots were used to characterise the internal water heat transfer coefficients (HTCs). A layer-by-layer (LbL) process was used to create the first nanostructured tube by coating the outside of a tube with silica nanoparticles. A chemical bath was used to create copper oxide (CuO) protrusions on the second nanostructured tube. The third tube was coated by following a commercial process referred to as nanoFLUX. R-245fa at a saturation temperature of 20 °C and R-134a at saturation temperatures of 5 °C and 25 °C were used as refrigerants. Tests were conducted over a range of heat fluxes from 20 to 100 kW/m and refrigerant mass flow rates per unit length from 0 to 0.13 kg/m/s, which corresponds to a film Reynolds number range of 0 to approximately 1500 to 2500, depending on the refrigerant. Heat fluxes were increased further to test whether critical heat flux (CHF) could be reached. The CuO and nanoFLUX tubes had the lowest film Reynolds numbers at which critical dryout occurred at heat fluxes near 20 kW/m^2, but as the heat fluxes were increased towards 100 kW/m^2, the critical dryout occurred at the highest film Reynolds numbers of the tubes tested. Furthermore, in some higher heat flux cases, the CHF point for the CuO and nanoFLUX tubes was reached before critical dryout occurred, and CHF became the limiting operational factor. The refrigerant condition that had the worst dryout performance in terms of film Reynolds number was R-134a at 25 °C, followed by R-134a at 5 °C and R245fa at 20 °C. Tests across the heat flux range and refrigerant conditions revealed that the roughened tube had HTCs between 60 to 100% higher, the LbL and CuO tubes had HTCs up to 20% higher, and the nanoFLUX tube had HTCs between 40 to 200% higher than the polished tube. The falling film enhancement ratios for the plain and nanostructured tubes were found to be of a similar order of magnitude, typically between 1.3 and 0.8.

Keywords

falling film evaporation, boiling, heat transfer coefficient, nanostructures, critical heat flux, dryout

* Corresponding author
Email address: josua.meyer@up.ac.za

Nomenclature

Symbols	
a	Fitting coefficient
C	Wilson plot modifier coefficient
c_p	Specific heat capacity
D	Diameter of tube
Γ	Refrigerant mass rate per unit length
h	Heat transfer coefficient
h^+	Normalised heat transfer coefficient
K	Enhancement ratio
L	Length of tube
$\dot{m}$	Mass flow rate
n	Fitting exponent
μ	Dynamic viscosity
p_r	Reduced pressure
q	Heat flux
R_a	Arithmetic mean roughness
R	Thermal resistance
Re_f	Film Reynolds number
T	Temperature
U	Overall heat transfer coefficient
x	Coordinate dimension along the length of the tube

Subscripts	
cr	Critical
evap	Evaporative limit
ff	Falling film
Gniel	Gnielinski correlation
i	Inner
o	Outer
pb	Pool boiling
pol	Polished
r	Liquid refrigerant
sat	Saturated refrigerant
surf	Surface enhancement relative to polished surface
w	Water
ws	Wall superheat
wall	Tube wall

Abbreviations	
AFM	Atomic force microscopy
CHF	Critical heat flux
CuO	Copper oxide
HTC	Heat transfer coefficient
LED	Light-emitting diode
LbL	Layer-by-layer
SEM	Scanning electron microscope
SiO_2	Silicon dioxide/Silica
TiO_2	Titanium dioxide

1. Introduction

Liquid falling films are important free-surface flows that have attracted considerable research attention since the late 1940s. These flows allow considerable heat transfer rates with low flow rates and low liquid volumes, as well as low pressure drops and, as such, play a key role in many thermal engineering applications. They have been investigated computationally and experimentally, from fundamental and applied perspectives [1-3], in external or internal flow systems with and without heat transfer, in the latter case in an effort to understand the emergence of different wave phenomena. Such waves are known to play a controlling role in affecting flow hydrodynamics and heat transfer [4-6] in simple film flows. The case of boiling films is even more complex and requires further attention, with studies of the boiling of stationery thin films [7,8] and thin falling films [9-11] having shown the importance of bubble nucleation and microlayer evaporation on the heat transfer process and the accompanying limitations of dryout and critical heat flux.

Horizontal falling film evaporators are used within the refrigeration industry and offer lower refrigerant charges than for flooded evaporators [12,13]. Especially for refrigerants this is an attractive alternative as it can reduce the impact of leaks to the environment and safety concerns regarding modern refrigerants, some of which are classified as mildly flammable (e.g. hydrofluoroolefins). But when insufficient liquid is supplied to prevent dry patches from forming, this dryout can be a concern due to the subsequent reduction in heat transfer [12,13]. Typically, falling film dryout occurs in two stages. Firstly, as the Γ_r is lowered from a high point, a plateau region is seen where HTCs remain relatively insensitive to changes [14,15] or slightly decrease [16,17] or slightly increase [18]. After this, a critical film Reynolds number is reached where HTCs decrease significantly when flow rates are decreased further [14-17] as a result of critical dryout. Higher heat transfer coefficients (HTCs) have been measured for falling film boiling of refrigerants than for pool boiling under identical conditions when boiling refrigerant on plain and micro-enhanced tubes but as heat fluxes are increased and refrigerant flow rates lowered, the HTCs of falling film boiling lower below their pool-boiling counterparts due to dryout [19-21]. The operational abilities of falling film evaporators are thus practically limited by dryout, both in the plateau region, where lowered HTCs can reduce performance, as well as critical dryout, where the HTCs are sharply reduced and the operational limit is effectively reached.

Nanostructured surfaces may be able to extend the operational limits of falling film evaporators. Some of these surfaces have been developed to have superhydrophilic wetting capabilities and many are wickable, drawing liquid into the surface through capillary action [22,23]. These nanostructured surfaces have delayed the onset of critical heat flux (CHF) in pool-boiling studies compared with plain surfaces, thought to be through mechanisms such as the improved wettability of the surfaces, surface wicking of liquid [22,23] or increased bubble contact line length [24], which may all contribute to the prevention of the formation of a stable vapour layer. This improved wetting ability thus offers an exciting opportunity for falling film boiling against dryout.

No literature has been found for the use of surfaces that can be categorised as nanostructured in falling film-boiling conditions. Reduced dryout compared with dryout for plain surfaces has been successfully achieved on 3D micro-enhanced and micro-porous tubes tested under falling film-boiling conditions with refrigerants, with plateau regions more insensitive to flow rate changes [16,17,25] and critical dryout at lower mass flow rates [16,17] than for plain tubes. The improved wetting performance has been suggested to be through the interconnected pores of the 3D micro-enhanced surfaces supplying and spreading liquid across the tube surface [16]. Horizontal tube falling film convective heat transfer studies of water at sub-atmospheric pressures have shown reduced dryout for superhydrophilic and hydrophilic tubes compared with dryout for a plain tube [26] and porous and hydrophilic tubes compared with dryout for a plain tube [27].

When testing superhydrophilic, hydrophilic and plain tubes with water, Zheng et al. [26] showed that under falling film convective heat transfer conditions, the HTCs were similar for all tubes tested as the film Reynolds number was decreased. Once the film Reynolds number dropped below a value of approximately 300, the HTCs for the plain tube decreased and the tube was seen to experience dryout, while the superhydrophilic and hydrophilic tube HTCs increased and were able to maintain a fully wetted surface under these low flow conditions. The resulting thin fluid film was thought to reduce the evaporative thermal resistance and cause the increased HTCs. A study by Lee et al. [28] also showed that micro-porous tubes improved wetting through capillary-assisted wicking of water in a falling film convective heat transfer study and as film Reynolds number was decreased, the micro-porous tube HTCs increased, while plain tube HTCs remained constant and then decreased due to dryout.

Recent studies have shown that falling film boiling typically follows a number of trends seen in pool boiling, with increased reduced pressure increasing HTCs in studies for plain and micro-enhanced surfaces [15,20,29,30], while increased roughness increases falling film-boiling HTCs and changes in material influence the HTCs in terms of the material's effusivity for plain tubes [30].

Pool-boiling heat transfer of nanostructures with organic fluids should offer some insight into the expected falling film-boiling performance, despite the relative sparseness of literature on the topic, which is evident in reviews of the topic [22,23,31-34]. Previous studies found that organic fluid pool-boiling HTCs were improved or worsened by the addition of nanostructures. Increased HTCs were attributed to increased surface roughness [35-38], while decreased HTCs seen by Trisaksri and Wongwises [39] in the pool boiling of a cylindrical copper tube in a R-141b/TiO_2 nanoparticle solution could be attributed to reductions in surface roughness, with the nanoparticles coating the surface and possibly reducing the number of active nucleation sites. Increased HTCs as a result of nanostructured surfaces in our previous study [40] were found to be through changes in the nucleation site density and additional unique mechanisms as a result of capillary flow of liquid through the nanoporous surfaces. This capillary liquid flow may have induced high single phase convective HTCs within the nanoporous coating as well as reduced dryout underneath nucleating bubbles resulting in increased microlayer evaporation.

The CHF of falling film boiling may also be a concern when nanostructures are used because the pool boiling of organic fluids on nanostructured surfaces has shown reduced CHF compared with that of plain surfaces [38,40-42]. Ueda et al. [43] provided an illustration of both critical dryout and CHF limitations for the falling film boiling of water and refrigerants R-11 and R-113 on the outside of vertical tubes. Critical dryout was noted where large stable dry patches were formed. CHF of the type seen in pool boiling where the fluid separated from the surface was also recorded with the fluid seen to lift from the surface with a thin liquid subfilm underneath. This subfilm, also noted in studies on vertical plates [11,44,45], was thought to be key to the process and it was theorised that falling film CHF occurred when that layer dried out. Ueda et al. [43] showed that falling film boiling could be limited by either critical dryout or CHF depending on conditions.

In this study, nanostructured tubes were investigated to determine their viability in terms of dryout and HTC for falling film boiling of refrigerants. Plain tubes were also investigated to better understand their operation under falling film-boiling conditions as well as to serve as a reference. HTCs were experimentally measured on one polished, one roughened and three nanostructured horizontal copper tubes under saturated falling film-boiling conditions on the outside of tubes internally heated by water. Tests were conducted in R-245fa at a saturation temperature of 20 °C and R-134a at saturation temperatures of 5 °C and 25 °C to allow for a wide range of reduced pressures within the

limits of the experimental equipment used, with respective reduced pressures of 0.034, 0.086 and 0.160. Heat fluxes ranged from 20 to 100 kW/m^2 and Γ_r on one side of the tube from 0 to approximately 0.13 kg/m/s, which corresponds to a film Reynolds number range of 0 to approximately 1500 to 2500, depending on the refrigerant. Heat fluxes were also increased above 100 kW/m^2 to see if CHF could be reached with the experimental apparatus. This study builds upon previous work by the same authors on falling film boiling over plain tubes in R-134a [30] and pool boiling over nanostructured tubes[40], with those results used and referenced in this study.

2. Experimental apparatus and tubes tested

2.1. Experimental apparatus

Bock et al. [30] gave a detailed description of the testing equipment and procedure and so they will only be described here in brief. Falling film-boiling studies were conducted with tubes placed horizontally into a test chamber with a thin film of refrigerant distributed along the length of the outside of the tubes. The tubes were heated internally by flowing water and individually tested.

The falling film of liquid refrigerant was conditioned by a liquid refrigerant loop, while the refrigerant vapour produced was condensed by a vapour refrigerant loop, both illustrated in Figure 1. The refrigerant vapour produced from the boiling in the test chamber was initially drawn downwards away from the boiling tubes so as not to obscure the falling film-boiling process and so that the vapour flowed concurrently with the falling film. This vapour flow was considered to have minimal influence on the falling film process because Ribatski and Thome [46] found that concurrent vapour flow of a velocity of approximately 1 m/s had little influence on falling film distribution or heat transfer and the maximum vapour velocity in this study was an order of magnitude smaller, calculated as 0.08 m/s.

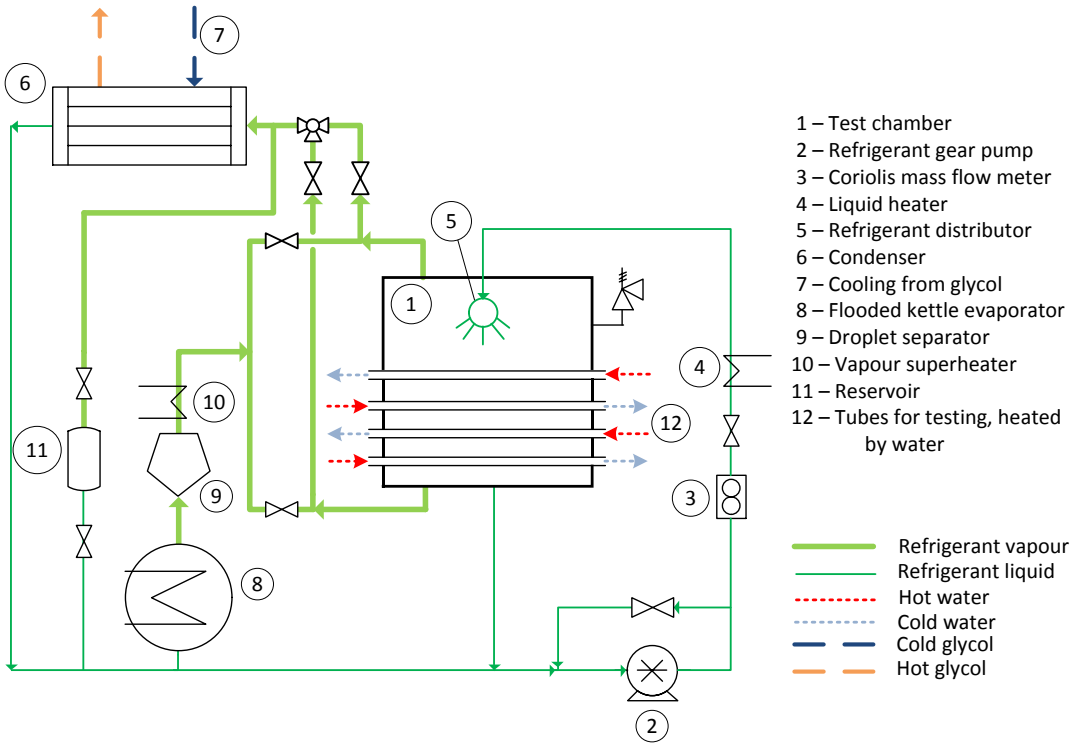

Figure 1. Schematic of the refrigerant loop with test chamber (from Ref. [30]).

The refrigerant saturation pressure was measured in the test chamber by both pressure transducers and thermocouples. These values were compared at start-up to ensure that minimal non-condensable gases were in the system. The heating water temperature profile within the tested tube was measured by a custom probe consisting of an 8 mm stainless steel tube with six thermocouples protruding into the heating water at three locations along the length of the tube.

The test chamber had windows on the front and back, which allowed a Photron FASTCAM Mini UX100 high-speed video camera with a Tonica AT-X 100 mm 2.8 macro lens and GS Vitec PT high-power white LEDs to capture images of the falling film-boiling process at 2 000 fps.

The maximum possible refrigerant flow rate per unit length, Γ_r, on a single side of a tube was approximately 0.13 kg/m/s across the range of conditions, with the maximum achieved Γ_r at each test condition of 0.14 kg/m/s for R-245fa at 20 °C, 0.13 kg/m/s and 0.12 kg/m/s for R-134a at 5 °C and 25 °C respectively. Tests were conducted where the Γ_r was kept at this maximum to minimise dryout and HTCs were measured as the heat flux was varied from 20 to 100 kW/m^2. The heat flux was initially raised at the start of testing above 100 kW/m^2 to ensure no hysteresis influence before beginning the tests at 20 kW/m^2. The heat fluxes were also raised above 100 kW/m^2 at the end of the test to determine whether CHF could be reached. Tests were also conducted at constant heat fluxes of 20, 50 and 80 kW/m^2 and the Γ_r was decreased from its maximum to the minimum value that could sustain the particular heat flux tested at.

2.2. Tubes tested

All tubes tested were copper and had an outer diameter of 19.05 mm (nominally ¾") and thickness of 1.2 mm with a heated length of 568 mm. A tube was polished with 1 200-grit sandpaper along the length of the tube to create a polished tube with a mean arithmetic roughness, R_a, of 0.12 μm measured across the grain with a Mitutoyo SJ Surftest 210 diamond tip profilometer. A tube was sanded with 40-grit sandpaper along the length of the tube to create a roughened tube with an R_a across the grain of 1.37 μm. Data from Bock et al. [30] of a 100-grit sandpapered tube with an R_a of 0.74 μm was also used in Section 5 as a roughened tube sample.

Three different nanocoatings were applied to the outside of copper tubes. The tubes were first polished with 1 200-grit sandpaper and cleaned with an ultrasonic probe in an acetone bath followed by a deionised water rinse.

The first nanocoating used a layer-by-layer (LbL) process developed by Rubner and Cohen [47] to apply LUDOX® TM-40 silica (SiO_2) nanoparticles with a diameter of approximately 20 nm to the surface of the tube. The tube was constantly rotated by an automated apparatus and dipped first into a cationic solution of poly (allylamine hydrochloride) followed by an anionic solution of silica nanoparticles with three deionised water rinses between each. Forrest et al. [48] gave a more detailed description of the process used in this study. This process was repeated 50 times to create a nominally 50 nanoparticle thick layer on the surface.

The second nanocoating process immersed a tube in an alkali oxidising solution heated to 95 °C for 10 min, which created copper oxide (CuO) nanostructures on the surface of the tube. The solution was detailed in Nam and Ju [49] and listed as the Type I solution. The tube was manually rotated at 1 min intervals to ensure an even distribution of nanostructures. The nanoFLUX© coating was the third nanocoating applied. This coating is a commercial process that was applied by Oxford nanoSystems.

Images from a scanning electron microscope (SEM) of samples taken around the circumference of the LbL and CuO tubes showed no discernible difference in surface structure, which proved that the coating process was applied uniformly around the tube.

The SEM images in Figure 2 illustrate the surface structure of the tubes. The polished (Figure 2 (a)) and roughened (Figure 2 (b)) surfaces showed longitudinal scratches of different sizes. The silica nanoparticles used to create the LbL surface are visible in Figure 2 (c). However, the nanoparticles appear to have clumped compared with previous studies that used the LbL coating [50,51], which was further confirmed by AFM images of the LbL surface, shown in Ref. [40]. The measured thickness of the LbL coating in Figure 2 (d) was approximately 0.4 to 0.5 μm. The CuO coating produced a mat of protrusions (Figure 2 (e)) with a thickness of approximately 2 to 3 μm. The nanoFLUX coating (Figure 2 (g)) also produced a mat of protrusions, but of a larger scale than for the CuO surface. The roughness of the nanocoatings could not be measured by the diamond tip profilometer as the tip scratched the surfaces. An atomic force microscope (AFM) was not able to characterise the CuO and nanoFLUX surfaces reliably due to their high aspect ratios.

The LbL and CuO coatings were so thin that they added no more than 0.1% to the thermal resistance of the tubes based on a calculated thermal resistance of the coatings with the layers assumed non-porous and composed only of silica and copper oxide respectively. Therefore, the influence of the nanocoatings on the wall thermal resistance was ignored.

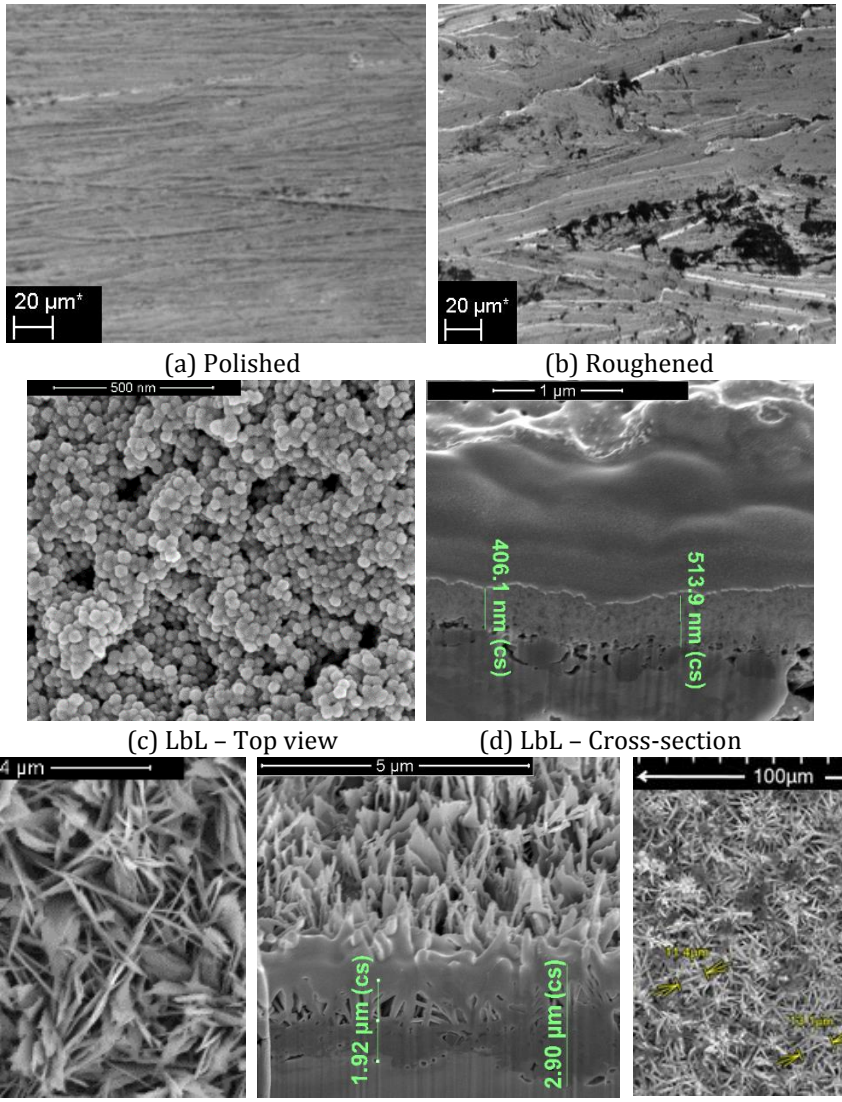

(a) Polished (b) Roughened

(c) LbL – Top view (d) LbL – Cross-section

(e) CuO – Top view (f) CuO – Cross-section (g) nanoFLUX©

Figure 2. SEMs of plain and nanostructured surfaces ((a) and (b) from Ref. [30], (c) to (g) from Ref.[40]).

The contact angles of distilled water in air are listed in Table 1 and were measured with a sessile drop contact angle tester at atmospheric conditions using a low-bond axisymmetric drop-shaped algorithm [52] implemented in the ImageJ software program [53]. The CuO surface was initially superhydrophilic with a contact angle of less than 5°, but after boiling in refrigerant for approximately two hours, its surface characteristics changed and stabilised as a hydrophobic surface likely in the Cassie-Baxter state with a contact angle of 122° with water. This was likely through the adsorption of the organic refrigerant onto its surface [54,55]. Thus, all surfaces were first boiled in refrigerant for a number of hours before testing began to ensure all surfaces were aged and stable. The nanoFLUX surface was also hydrophobic and likely in the Cassie-Baxter state, with air trapped in the nanostructure resulting in the poor wetting of the surface.

Table 1. Contact angles of aged surfaces.

Surface	Average contact angle (Average ± standard deviation) [°]
Polished	78 ± 4
Roughened	85 ± 3
LbL	52 ± 7
CuO	122 ± 24
nanoFLUX	161 ± 16

The contact angles of refrigerant in air at atmospheric conditions were measured with R-245fa and recorded with the high-speed video camera. Contact angles of approximately 20° were measured for all surfaces. The atmospheric temperature of 25 °C meant that significant evaporation took place as droplets were placed onto the surfaces and the droplets moved as a result, which introduced significant noise to the process. Therefore, discernible differences in contact angle between the surfaces could not be measured with this technique and refrigerant. However, all surfaces were wetted by the refrigerant and were likely in the Wenzel state.

The CuO and nanoFLUX surfaces were shown to wick liquid due to their porous nanostructures. This was confirmed with adiabatic tests where drops of refrigerant were seen to create a wicking front when placed onto the surface in saturated conditions within the test chamber. This was further confirmed with high-speed images of the falling film-boiling process, shown and discussed later in Section 5.2. No such wicking was seen for the polished, roughened or LbL surfaces.

3. Data reduction and uncertainty

A brief overview of the data reduction and calculated uncertainties are given here, with further details available in Bock et al. [30].

3.1. Data reduction

The local heat flux at the midpoint of the tube, q, was calculated according to Christians [56] as follows:

$$q = \frac{\dot{m}_w c_{p,w}}{\pi D_o} \frac{\mathrm{d}T_w}{\mathrm{d}x} \tag{1}$$

where D_o was the measured outer diameter of the tube, $\dot{m}_w$ was the measured mass flow rate of the heating water and the temperature gradient of the heating water along the length of the tube, $\mathrm{d}T_w/\mathrm{d}x$, was estimated at the midpoint of the tube using a second-order polynomial fit to the measured temperatures along the length of the tube.

All properties of the refrigerant and heating water, such as the specific heat capacity of the heating water, $c_{p,w}$, were estimated using REFPROP 8 [57] based on the measured temperature of the particular fluid.

The internal HTC, h_i, was determined through a Briggs and Young-type Wilson plot as implemented by Van Rooyen et al. [58]. h_i was assumed to take the form of the Gnielinski correlation [59], h_{Gniel}, with a lead coefficient, C_i, calculated from the Wilson plot to account for the presence of the temperature probe within the tube and correlation error as follows:

$$h_i = C_i h_{Gniel} \tag{2}$$

The overall HTC, U_o, was calculated at the midpoint of the tube as follows:

$$U_o = \frac{q}{T_w - T_{sat}} \tag{3}$$

where T_w was the estimated temperature of the water at the midpoint of the tube based on the second-order polynomial fit to the measured temperatures along the length of the tube and T_{sat} was the saturation temperature estimated with REFPROP 8 based on the measured saturation pressure of the refrigerant.

The external HTC, h_o, at the midpoint of the tube was thus calculated as follows:

$$h_o = \left(\frac{1}{U_o} - R_{wall} - \frac{1}{h_i}\frac{D_o}{D_i}\right)^{-1} \tag{4}$$

where R_{wall} was the calculated wall thermal resistance and D_i was the measured inner diameter of the tube.

The surface enhancement ratio relative to a polished tube, K_{surf}, was calculated as follows:

$$K_{surf} = \frac{h_o}{h_{o,pol}} \tag{5}$$

where $h_{o,pol}$ was the external HTC of the polished tube.

The falling film heat transfer enhancement ratio, K_{ff}, was calculated as follows:

$$K_{ff} = \frac{h_{o,ff}}{h_{o,pb}} \tag{6}$$

where $h_{o,ff}$ and $h_{o,pb}$ were the external HTCs under falling film-boiling and pool-boiling conditions respectively. The pool-boiling HTCs used in this paper were described in Ref. [40].

The refrigerant mass flow rate per unit length, Γ_r, was calculated for one side of the tube as follows:

$$\Gamma_r = \frac{\dot{m}_r}{2L} \tag{7}$$

where $\dot{m}_r$ was the total measured mass flow rate of the liquid refrigerant film supplied to the tube and L was the measured length of the tube. The film Reynolds number, Re_f, for one side of the tube was calculated as follows:

$$Re_f = \frac{4\Gamma_r}{\mu_r} \tag{8}$$

where the dynamic viscosity of the liquid refrigerant, μ_r, was estimated using REFPROP 8.

A normalised HTC, h^+, was calculated for studies where the Γ_r varied at a constant heat flux as follows:

$$h^+ = \frac{h_o}{h_o\,(Re_f=1250)} \tag{9}$$

where the h_o at a film Reynolds number of 1250 was used as the normalising denominator, as this was the highest film Reynolds number achieved under all refrigerant conditions.

The critical dryout limit was characterised by decreasing the film Reynolds number and noting when a sharp decline in HTC occurred due to dryout. This was previously identified in Bock et al. [30] by the point at which the gradient of the HTC versus film Reynolds number, $\mathrm{d}h_o/\mathrm{d}Re_f$, first went below 5 W/m²K as the film Reynolds number was increased. This approach struggled with some of the data generated in this study, particularly the HTC hump and the high HTC data of the nanoFLUX tube. The approach was refined to use the gradient of the normalised HTC, h^+, against the film Reynolds number. The critical dryout limit was thus defined as the first point, as the film Reynolds number was decreased from the maximum to the minimum recorded, at which all subsequent normalised HTC gradient points met the criteria as follows:

$$\frac{\mathrm{d}h^+}{\mathrm{d}Re_f} > 0.0005 \tag{10}$$

The CHF limit was determined in two ways, depending on the test conducted. In tests where the heat flux was increased and the Γ_r was kept constant at a maximum (typically 0.13 kg/m/s), the CHF limit was recorded as the highest heat flux obtained if liquid separation occurred. In tests where the heat flux was kept constant and the refrigerant film mass flow decreased, the CHF thus occurred at low flow densities, which resulted in immediate collapse of the heat flux and HTC. This CHF limit was thus the last data point successfully recorded at that heat flux before the onset of CHF if liquid separation was noted.

The critical film Reynolds number, $Re_{f,cr}$, was determined as the highest film Reynolds number at a particular heat flux at which either critical dryout or CHF occurred. This was needed for cases where further reductions in refrigerant mass flow resulted in CHF liquid separation after critical dryout occurred.

The evaporative limit, which is the minimum film Reynolds number that can support a particular heat flux assuming all supplied liquid is vaporised by the boiling process, was calculated as follows:

$$Re_{evap} = 4\pi D_o \frac{q}{h_{fg}\mu_l} \tag{11}$$

3.2. Uncertainty

The methodology of Dunn [60] was used to calculate the expanded standard uncertainties of the various sensors. The average expanded uncertainty of the temperature probes was 0.1 K, that of the pressure probes was 0.2%, that of the mass flow rate of water, $\dot{m}_w$, was 0.2% and that of the Γ_r was 0.3%. JCGM 100:2008 [61] was used to calculate the

combined standard uncertainties of the calculated quantities through the law of propagation of uncertainty. These uncertainties varied across the heat flux range and are summarised in Table 2.

Table 2. Summary of uncertainties.

	Overall average uncertainty	Average uncertainty at 20 kW/m²	Average uncertainty at 100 kW/m²
q	11%	26%	5.3%
h_o	31%	48%	23%
K_{ff}	3.2%	7.4%	2.0%

4. Critical heat flux

CHF occurred during testing of the CuO and nanoFLUX nanostructured surfaces. Tests that achieved CHF at the maximum Γ_r of the experimental apparatus of approximately 0.13 kg/m/s are illustrated in Figure 3 with the CHF point indicated by an arrow. CHF was also recorded in some instances for the CuO and nanoFLUX tubes in tests where the Γ_r was reduced and these instances are indicated with arrows in Figure 5.

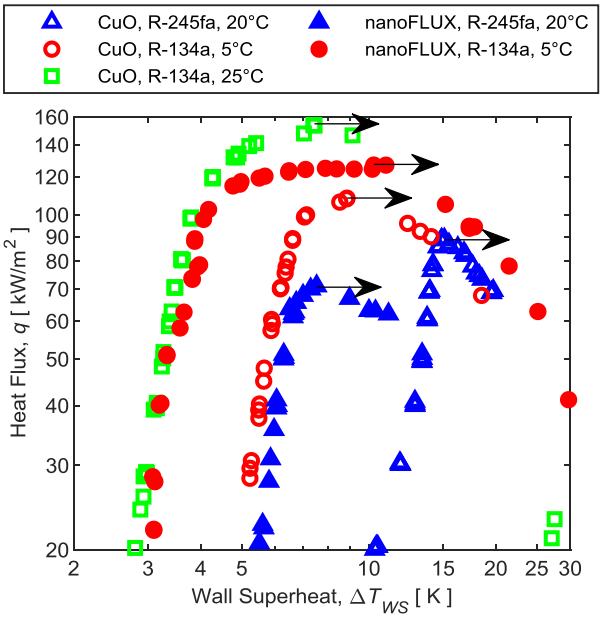

Figure 3. Heat flux versus wall superheat illustrating CHF of nanostructured tubes.

Increased wall superheat resulted in increased heat flux before the CHF point was reached. As the CHF point was approached, separation between the surface and liquid film was seen, initially at the inlet end of the tube. The liquid separation progressively moved along the length of the tube as wall superheat was further increased resulting in heat flux peaking and then decreasing because of the decreased proportion of the tube in contact with the liquid. The CHF eventually enveloped the entire tube with heat fluxes then collapsed to values below 10 kW/m², not shown in Figure 3. The heat fluxes of the plain and LbL surfaces were set to the maximum limit that the experimental equipment could support but no CHF could be obtained.

Images from the high-speed video camera illustrating the CHF liquid separation process are shown in Figure 4, taken at the midpoint of the tube length.

As the CHF point was approached at a particular point on the tubes, the falling film began to separate from the tube. The separation started at the bottom of the tube and moved up the tube circumference until the fluid was completely separated from the tube. The tube was no longer wetted by the fluid and the falling liquid film bounced off the tube and deflected around it. It should be noted that the images in Figure 4 were taken at the midpoint of the tube, while the liquid separation first began at the water inlet end of the tube. Thus, while the tube was fully wetted, as shown in Figure 4 (a,i) and (b,i), the water inlet end of the tube was already experiencing film separation.

Studies of falling film boiling on plain flat plates and vertical tubes [11,43-45] noted that liquid separation began at the bottom end of the heater plate or vertical tube, similar to this study. However, the studies of flat plates and vertical tubes noted the presence of a thin subfilm of liquid beneath the main separated liquid film and theorised that

this subfilm played a key role in the falling film CHF process. However, no subfilm was seen in this study, suggesting that this CHF took place through a different mechanism.

The CHF measured for the nanostructured surfaces was lower than that of a plain surface. For example, the polished surface was able to reach 100 kW/m^2 in R-245fa at 20 °C, above the 71 kW/m^2 CHF point of the nanoFLUX tube. Unfortunately, the CHF point of the plain and LbL tubes could not be reached as tests could not be conducted at higher fluxes due to the low HTCs of the plain and LbL tubes and the wall superheat limitations of the experimental equipment. The falling film CHFs were also lower than those recorded under pool-boiling conditions in our previous study with the same tubes and identical refrigerant conditions [40], as indicated in Table 3. The falling film CHFs were only about 50 to 60% of the respective pool-boiling values.

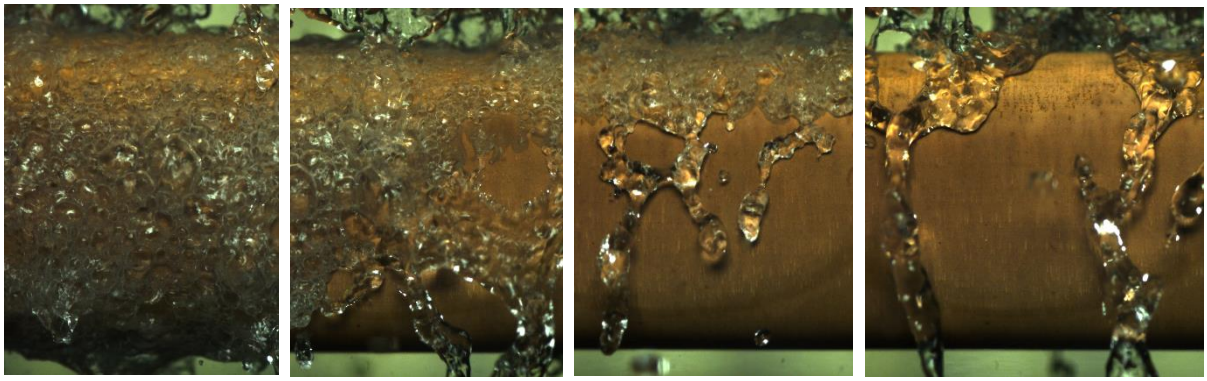

(i) ΔT_{ws} = 10 °C (ii) ΔT_{ws} = 15 °C (iii) ΔT_{ws} = 25 °C (iv) ΔT_{ws} = 42 °C

(a) nanoFLUX tube in R-134a at 5 °C at Γ_r of 0.13 kg/m/s.

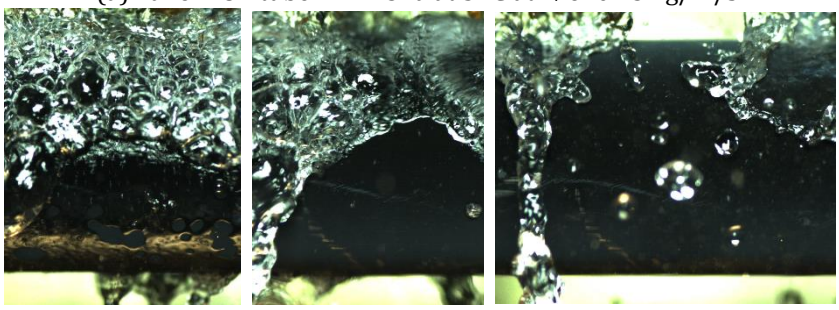

(i) ΔT_{ws} = 6.4 °C (ii) ΔT_{ws} = 14 °C (iii) ΔT_{ws} = 30 °C

(b) CuO tube in R-245fa at 20 °C at Γ_r of 0.14 kg/m/s.

Figure 4. Images of CHF liquid separation at midpoint of tube length.

Table 3. Measured CHF and comparison with pool-boiling CHF.

Condition	Surface	CHF_{ff} [kW/m^2]	CHF_{pb} [kW/m^2] (from Ref. [40])	$\frac{CHF_{ff}}{CHF_{pb}}$
R-245fa at 20 °C	nanoFLUX	71	112	0.63
	CuO	89	N/A	
R-134a at 5 °C	nanoFLUX	127	245	0.52
	CuO	108	189	0.57
R-134a at 25 °C	CuO	154	N/A	N/A

Figure 4 (a,ii) shows that the nanoFLUX and CuO surfaces experienced this early CHF despite wicking still taking place on the upper section of the tube, while separation was occurring on the bottom half of the tube. The early onset of CHF was possibly caused by the same mechanism as proposed in our pool boiling study [40], namely once the wicking was overcome and the nanostructures dried out, a Cassie-Baxter state of wetting was initiated (a likelihood illustrated by the water contact angle data) and thus an early onset of CHF compared to plain tubes.

5. Dryout

5.1. Heat transfer as a function of refrigerant mass flow rate

The influence of the Γ_r on the HTCs of the polished, roughened and nanostructured tubes is shown in Figure 5. As the Γ_r was decreased, both plain and nanostructured tubes displayed a relatively insensitive HTC response, resulting in the typical plateau region. The sensitivity of the plateau region increased as the heat flux was increased for most tubes, particularly for the plain tubes. Dry patches were observed within these plateau regions with the aid of the high-speed camera. These patches were temporary and quickly covered by the flowing liquid film, as noted in previous studies [46].

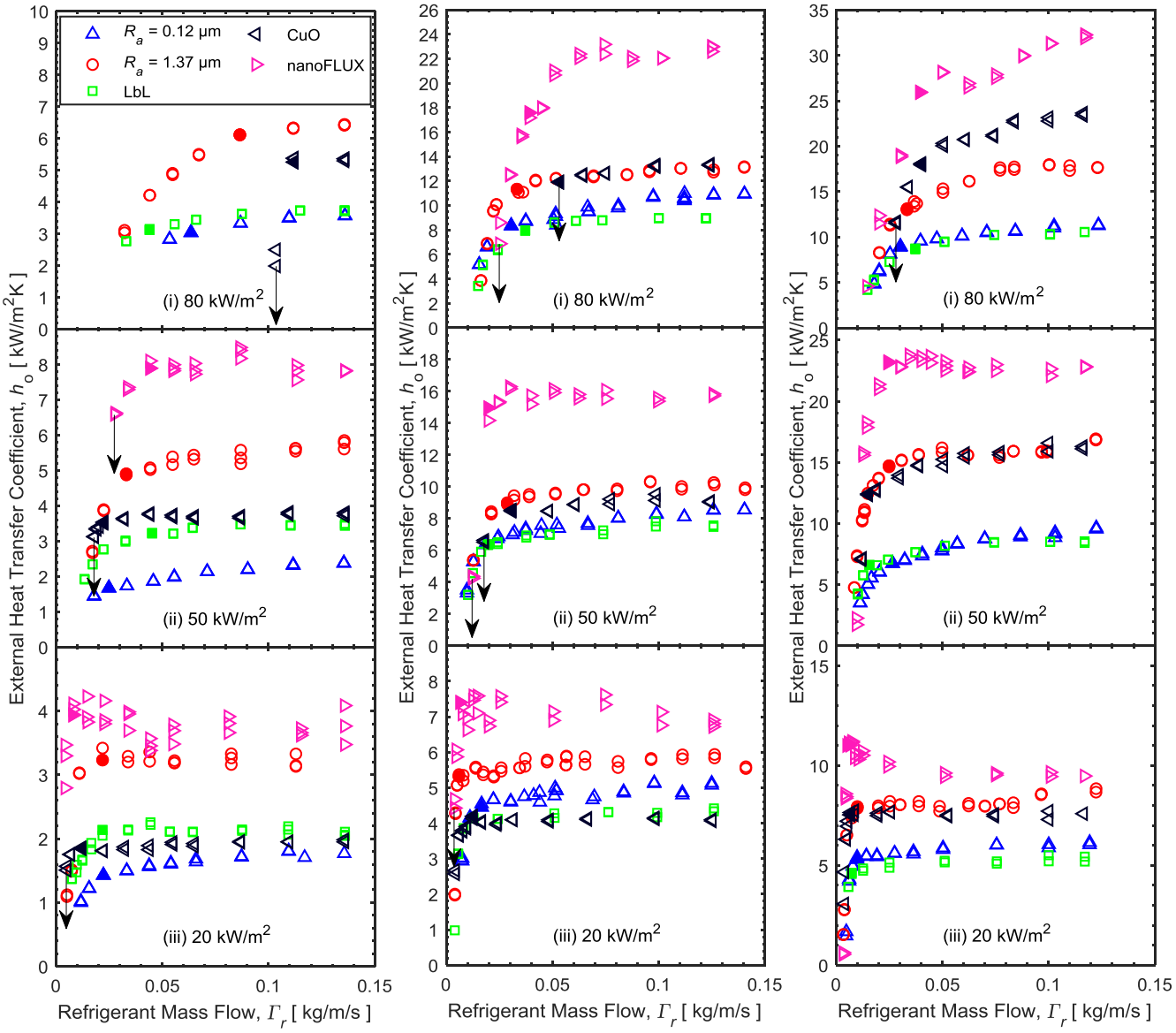

(a) R245fa, 20 °C, p_r 0.034 (b) R134a, 5 °C, p_r 0.086 (c) R134a, 25 °C, p_r 0.160

Figure 5. HTCs as a function of Γ_r (Polished and roughened data for R-134a at 5 °C taken from Bock et al. [30]). Critical dryout indicated by filled-in markers.

The HTCs collapsed as refrigerant mass flow was reduced further for both the plain and nanostructured tubes. This was caused by critical dryout, with the formation of large dry patches visible on the tube surfaces and insufficient liquid flow available to rewet the dry patches, while liquid boiled on the wetted portions of the tubes. The point of critical dryout is noted by filled-in markers in Figure 5. This critical dryout was seen to occur at higher flow densities as the heat flux was increased for both plain and nanostructured tubes.

CHF was seen on the CuO and nanoFLUX tubes in a number of cases as the Γ_r was decreased, which resulted in the separation of the fluid from the tube surface and led to almost instantaneous decrease in HTC as the tube was no longer wetted and no boiling could take place. CHF cases are noted in Figure 5 with a downward arrow. However, a number of these cases occurred after the Γ_r was below the critical dryout point. In these cases, critical dryout was the limiting factor rather than the CHF because the HTCs had decreased significantly already.

The nanoFLUX tube displayed an increase in HTC as Γ_r was decreased in some cases, for example in R-134a at 25 °C at 20 kW/m^2, as shown in Figure 5 (c,iii), resulting in an HTC 'hump'. This phenomenon of increased HTC at reduced falling film flow density was captured before in the convective heat transfer of water falling films on Gewa-T 3D micro-enhanced tubes [62] and superhydrophilic and hydrophilic tubes [63]. This was also seen in the falling film boiling of refrigerants on micro-enhanced tubes in R-134a [16,18]. A thinned liquid layer, which resulted in a decrease in evaporative thermal resistance, was considered the likely cause [62,63].

Images of the boiling process during the increased HTC hump are shown in Figure 6. The HTC hump occurred at Γ_r of 0.02 kg/m/s, as shown in Figure 6 (b), with a completely wetted surface with very little waves or rivulets compared with the higher flow density, as shown in Figure 6 (a), supporting the idea of a stable thin layer being formed. Furthermore, the backlight below the tube where the vapour passed, as shown in Figure 6 (b), was the darkest, which again suggested that significant evaporation of fluid was taking place, increasing the HTCs. The HTC dropped rapidly after Γ_r was further decreased through the formation of stable dry patches visible in Figure 6 (c). The nanoFLUX tube had to maintain a film layer so thin that the evaporative thermal resistance became so low that it could meaningfully contribute to the HTC thus causing the hump, because previous reductions in film thickness at higher Γ_r were not accompanied by increased HTCs.

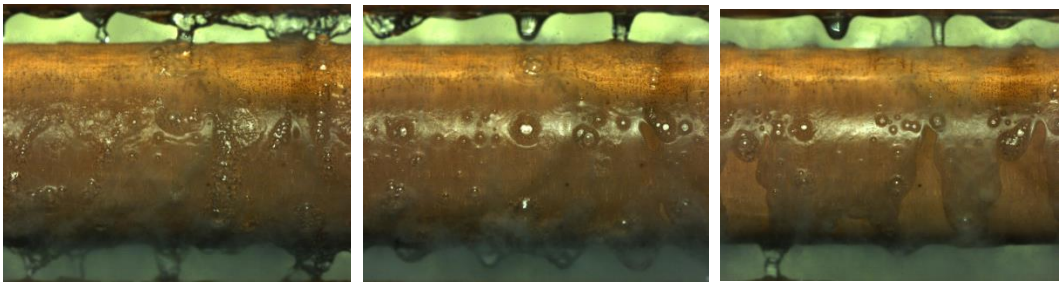

(a) Γ_r of 0.1 kg/m/s (b) Γ_r of 0.02 kg/m/s (c) Γ_r of 0.01 kg/m/s

Figure 6. Heat transfer hump for nanoFLUX tube in R-134a at 25 °C at 20 kW/m^2.

In an effort to understand the influence of surface and refrigerant properties on dryout, a normalised HTC , h^+, and the dimensionless film Reynolds number, Re_f, were plotted for 50 kW/m^2, as shown in Figure 7. The plateau region of the polished tube was the most sensitive to film Reynolds number changes. The nanoFLUX tube and to a lesser degree the CuO tube had plateau regions that were very insensitive to film Reynolds number changes. The roughened and LbL tubes had plateau regions of intermediate film Reynolds number sensitivities.

The differing sensitivities of the surfaces could be through intermittent dryout. While the dry spots which formed within the plateau region were temporary, these dry spots would still temporarily reduce the heat transfer and thus have a negative effect on the time-averaged HTC. Surfaces with lower wettability could have a greater frequency of intermittent dry spots than surfaces with a higher wettability. The frequency of intermittent dry spots was expected to increase as the film Reynolds number was decreased thus having a progressively more negative effect on the HTCs of affected surfaces. Image analysis of these intermittent dry spots would be a recommended method of determining if this indeed was the case.

Figure 7 shows that at a given film Reynolds number, the normalised HTC was typically the lowest for R-134a at 25 °C, followed by R-134a at 5 °C and then R-245fa at 20 °C across all tubes tested. Therefore, on a film Reynolds number basis, HTCs in R-134a at 25 °C were most negatively affected by dryout, followed by R-134a at 5 °C and then R-245fa at 20 °C.

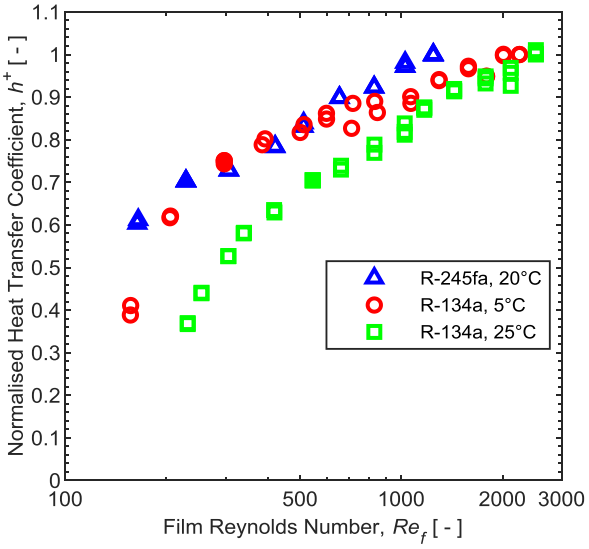

(a) Polished

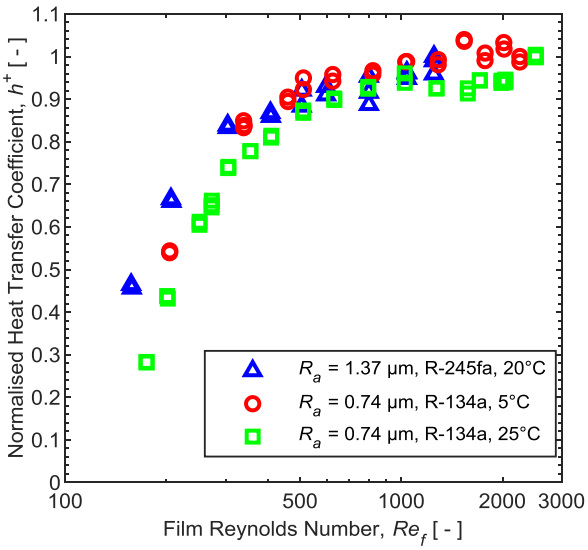

(b) Roughened

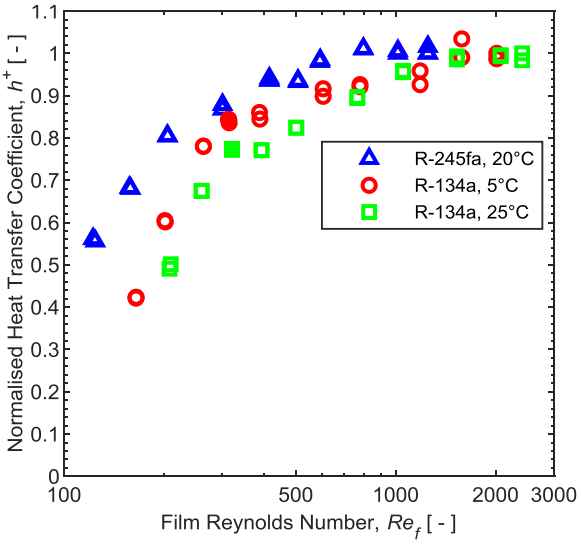

(c) LbL

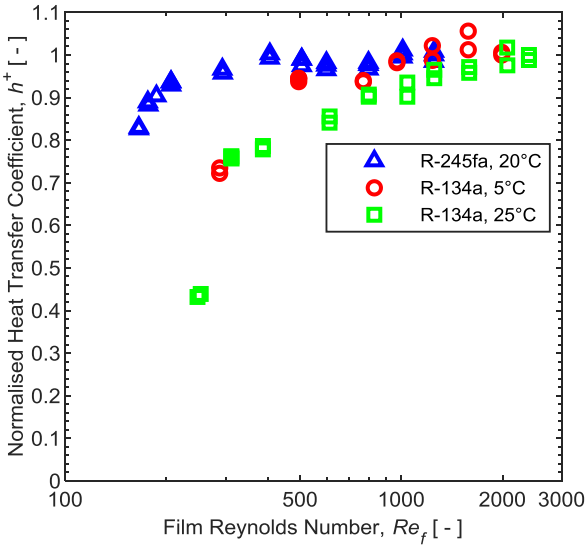

(d) CuO

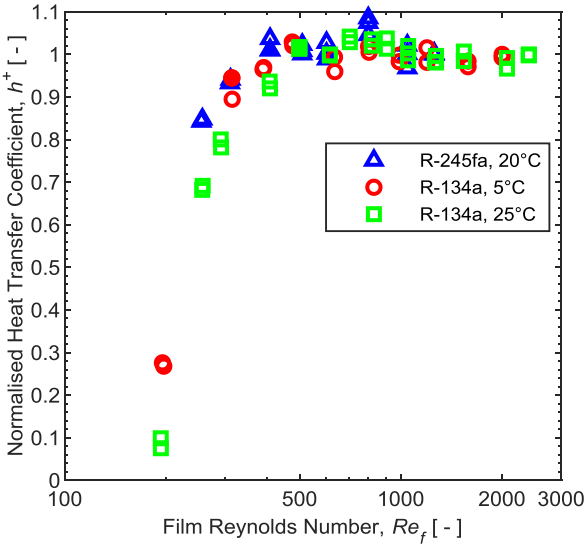

(e) nanoFLUX

Figure 7. Normalised HTC versus Re_f at 50 kW/m². Critical dryout point indicated with filled markers.

5.2. Dryout mechanisms

Figure 8 shows a zoomed-in progression of a dry spot on the polished and nanoFLUX tube in R-245fa at 20 °C at 50 kW/m^2. Figure 8 (a) indicates that a dry spot was started on the polished tube by a bubble popping, just before the frame began. The dry spot increased in size and then merged with a neighbouring dry spot. As the two dry spots merged, necking could be seen between the two spots, as indicated by the arrows at t = 7 ms. No wicking was visible in these images for the polished tube. A dry spot began on the nanoFLUX surface with a thinned region, indicated by arrows in Figure 8 (b) at the 0 and 3.5 ms mark. As the dry spot grew, a small wicking front could be seen around the dry spot. A larger wicking front appeared once the dry spot merged with a neighbouring dry spot at the 17.5 ms mark, indicated by arrows.

t = 0 ms t = 2.5 ms t = 7 ms t = 11 ms t = 14 ms t = 17.5 ms

(a) Polished

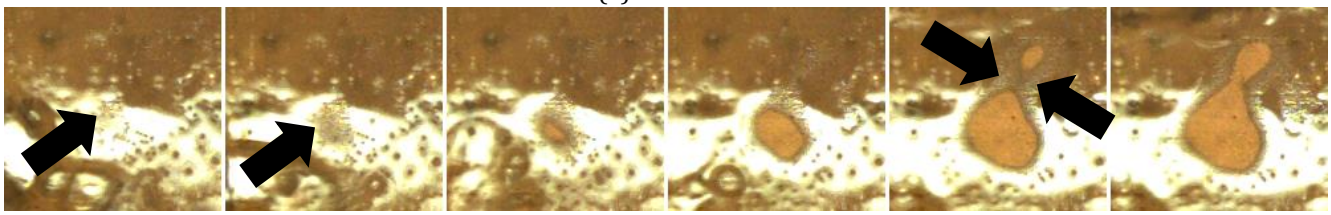

t = 0 ms t = 3.5 ms t = 6 ms t = 10.5 ms t = 17.5 ms t = 19 ms

(b) nanoFLUX

Figure 8. Dry spot progression of polished and nanoFLUX tubes in R-245fa at 20 °C at 50 kW/m^2.

The difference between the polished tube and nanoFLUX tube wetting ability was not evident from the refrigerant or water contact angles measured, but with wicking confirmed to take place on the nanoFLUX tube, as illustrated in Figure 8. It was likely the reason for the insensitive plateau region of the nanoFLUX tube and the ability to maintain a thin stable film at low Γ_r, resulting in the increased HTC hump seen under some conditions.

6. Operational limits

The operational limits of the tubes are illustrated in Figure 9 with the critical film Reynolds number as a result of critical dryout (open markers) or CHF (filled markers) as a function of heat flux. The evaporative limit for each respective refrigerant condition was also plotted.

Lower heat fluxes resulted in lower film Reynolds numbers at which critical dryout or CHF occurred. Higher flow densities suppressed critical dryout, with the liquid film rewetting dry spots that formed. Similarly, higher flow densities suppressed CHF, with the falling liquid likely suppressing the dryout of the nanostructures and preventing the separation of the liquid film from the surface.

The critical film Reynolds numbers were the lowest for R-245fa at 20 °C, while R-134a at 25 °C had slightly higher critical dryout limits than for R-134a at 5 °C. This agrees with the trends in Figure 7 in terms of rate at which the normalised HTC, h^+, decreased as film Reynolds number was decreased, where R-134a at 25 °C had the earliest normalised HTC drop, followed by R-134 at 5 °C and then R-245fa at 20 °C.

The polished tube had some of the highest film Reynolds numbers at which critical dryout occurred at a heat flux of 20 kW/m^2, while the CuO and nanoFLUX tubes had some of the lowest. As the heat fluxes were increased above 20 kW/m^2, the critical film Reynolds number increased for the CuO and nanoFLUX surfaces by the greatest amount of all the tubes such that they were the highest at 80 kW/m^2. At approximately this heat flux, CHF now became a concern and at times, the limiting factor for the CuO and nanoFLUX surfaces.

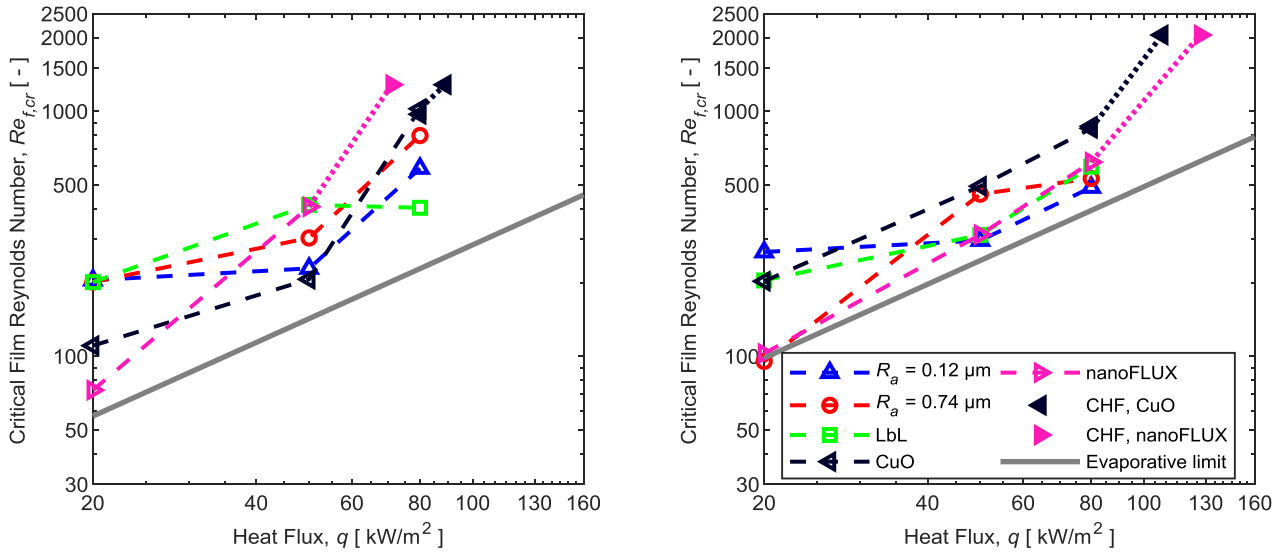

(a) R-245fa, 20 °C, p_r of 0.034

(b) R-134a, 5 °C, p_r of 0.086

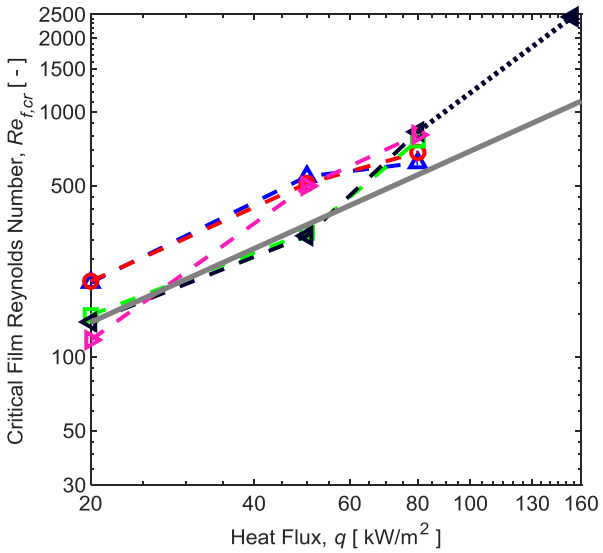

(c) R-134a, 25 °C, p_r of 0.160

Figure 9. Critical film Reynolds number as a function of heat flux.

The CuO and nanoFLUX surfaces were thus shown to provide good dryout resistance at low heat fluxes (~ 20 kW/m²) but at increased heat fluxes (~ 80 kW/m²), these surfaces had poor critical dryout resistance and poor CHF resistance. The worsened dryout and CHF performance of the CuO and nanoFLUX surfaces were possibly through the dryout of the underlying nanostructures and subsequent operation in the Cassie-Baxter state of wetting, resulting in poor wetting and thus poor critical dryout and CHF performance.

However, the normalised HTC data of Figure 7 should be kept in mind when considering the dryout limits, as shown in Figure 9. For example, the polished tube HTCs dropped by between 20 to 30% at a film Reynolds number of 500 at 50 kW/m² across the conditions tested, while the nanoFLUX tube still had HTCs within 3% of its maximum HTC. This merits consideration from designers of falling film evaporators, as both surfaces have critical dryout limits below a film Reynolds number of 500, but the high sensitivity of tubes such as the polished surface means that significant HTC reduction can take place within the plateau region.

7. Heat transfer

7.1. Heat transfer coefficients

The HTCs measured during falling film boiling of the polished, roughened and three nanostructured tubes are shown in Figure 10 at a Γ_f of approximately 0.13 kg/m/s at three reduced pressures. All tubes showed a linear increase in HTCs as heat flux was increased on the log-log plot.

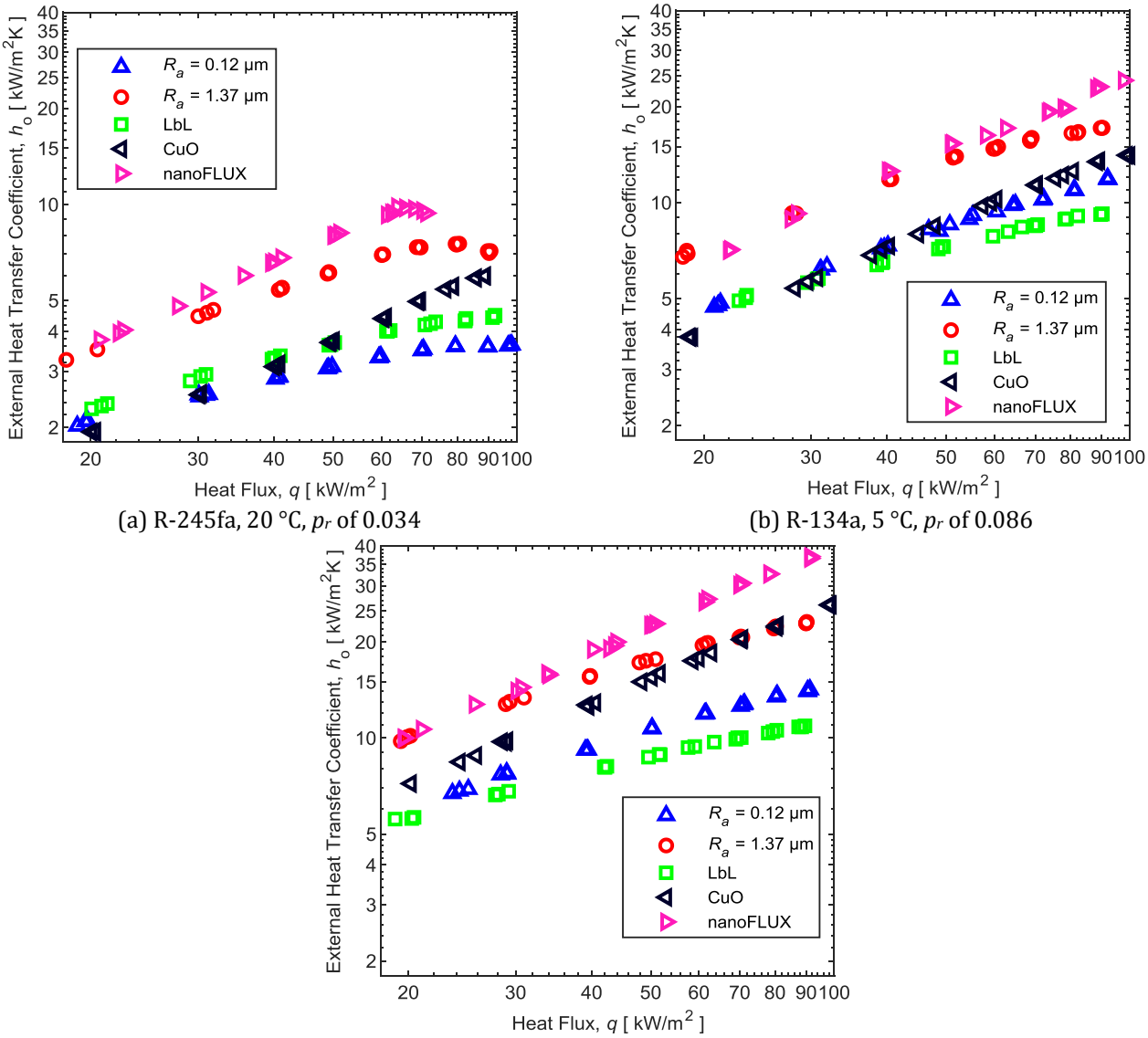

(a) R-245fa, 20 °C, p_r of 0.034

(b) R-134a, 5 °C, p_r of 0.086

(c) R-134a, 25 °C, p_r of 0.160

Figure 10. HTCs as a function of heat flux at different reduced pressures with a Γ_r of approximately 0.13 kg/m/s (Polished and roughened tube data for R-134a taken from Ref. [30]).

However, at a reduced pressure of 0.034, the gradient of the HTCs of some surfaces began to decrease as heat fluxes approached the upper end of the heat flux range tested. This was caused by dryout for the polished and roughened surfaces and CHF for the nanoFLUX surface, as previously discussed. The polished and LbL tubes recorded the lowest HTCs across the three reduced pressures, the roughened and nanoFLUX tubes recorded the highest HTCs and the CuO surface HTCs were intermediate.

The polished tube was used as a baseline to better illustrate the performance of the nanostructured tubes through the surface enhancement ratio in Figure 11. The roughened tube HTCs outperformed the polished tube HTCs by approximately 60% at the highest two reduced pressures and reached a maximum of 100% higher HTCs at the lowest reduced pressure. The LbL tube at a reduced pressure of 0.034 outperformed the polished tube by up to 20% but at the higher reduced pressures, the HTCs were 20% lower. The CuO tube HTCs were 20% lower than the polished tube HTCs at the lower range of the heat fluxes, but between 60 to 80% higher at the upper end of the heat flux range. The nanoFLUX tube had HTCs between 40 to 80% higher than those of the polished tube at the lower end of the heat flux range and up to 200% higher HTCs at the upper end of the heat flux range. Therefore, both the CuO and nanoFLUX tubes had increased sensitivity to heat flux changes compared with the polished tube.

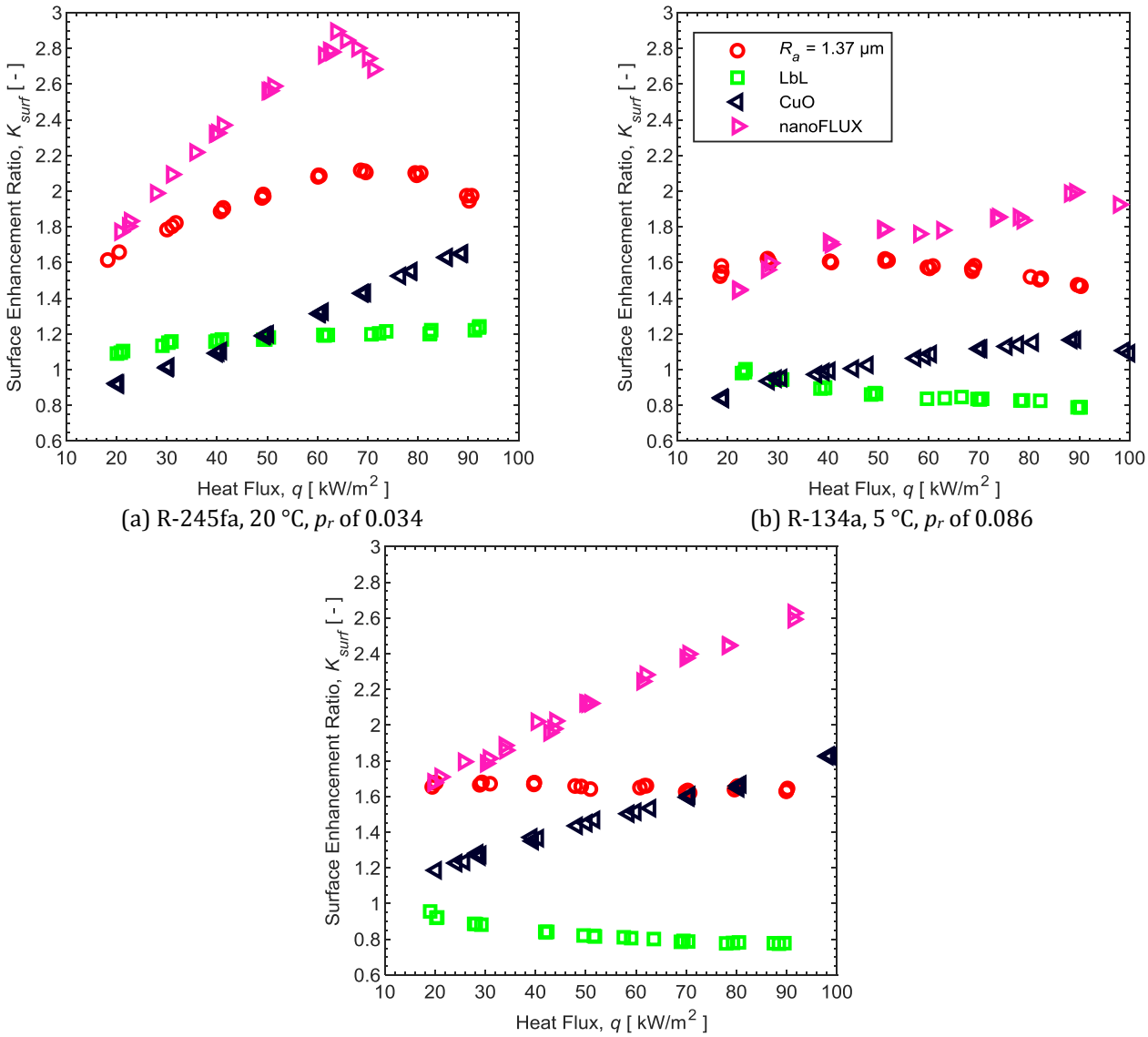

(a) R-245fa, 20 °C, p_r of 0.034

(b) R-134a, 5 °C, p_r of 0.086

(c) R-134a, 25 °C, p_r of 0.160

Figure 11. HTC performance relative to smooth polished tube as a function of heat flux.

This increased sensitivity was further investigated by fitting the relation $h_o = aq^m$ to the data of Figure 10 with the results in Figure 12 (a). The heat flux sensitivities of the smooth, roughened and LbL tubes were similar, with an m of approximately between 0.4 to 0.6, while the CuO and nanoFLUX were more sensitive to heat flux changes with an m of approximately 0.8. This was similar to the pool-boiling results seen in our pool-boiling paper [40], which suggested that the CuO and nanoFLUX tubes had a higher number of smaller nucleation cavities that were activated under both pool-boiling and falling film-boiling conditions as heat fluxes were increased compared with the other tubes.

In order to quantify the influence of liquid properties, the HTCs were plotted against the reduced pressure at 50 kW/m^2, as shown in Figure 12 (b). The HTC of all tubes increased as the reduced pressure was increased, as indicated in the corresponding pool boiling results [40]. The CuO and nanoFLUX tubes showed a linear increase in HTC on the plot, while the polished, roughened and LbL tubes showed a reduction in the gradient as the reduced pressure reached its maximum. This may again be a result of a large population of small nucleation cavities that were activated as reduced pressure increased or as a result of dryout at the highest reduced pressure, which influenced the nanoFLUX and CuO plateau region the least.

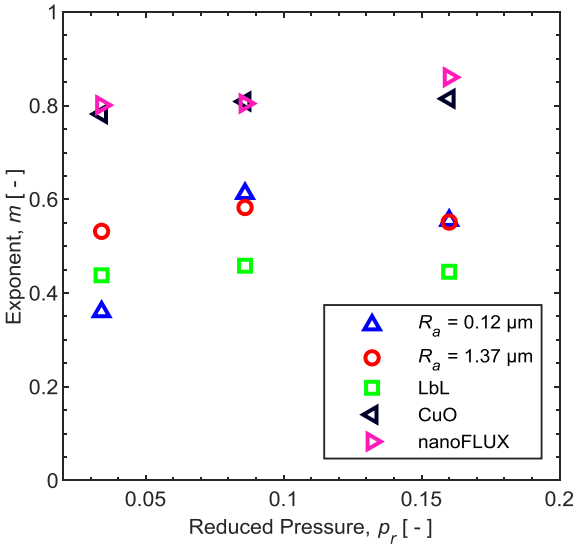

(a) Fitted exponent, m

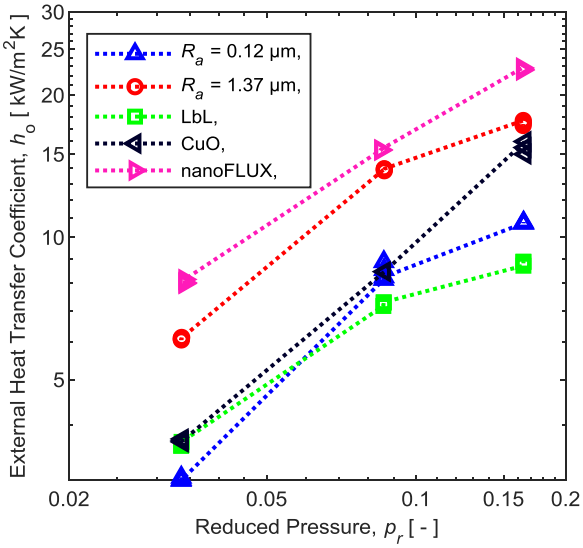

(b) HTCs at 50 kW/m^2

Figure 12. Influence of reduced pressure on HTCs and coefficient m.

7.2. Nucleation site density

In an attempt to quantify the nucleation site density of the surfaces, images from the high-speed camera were taken at the lowest HTCs and thus lowest expected nucleation site density in R-245fa at 20 °C and these are shown in Figure 13. Nucleation sites could not be counted as was done for the pool-boiling case in Ref. [40] because nucleation primarily occurred at the top of the tube with limited nucleation on the sides of the tube. The bubbles slid down the tube, which also obscured the sidewall nucleation sites more than was the case for pool boiling.

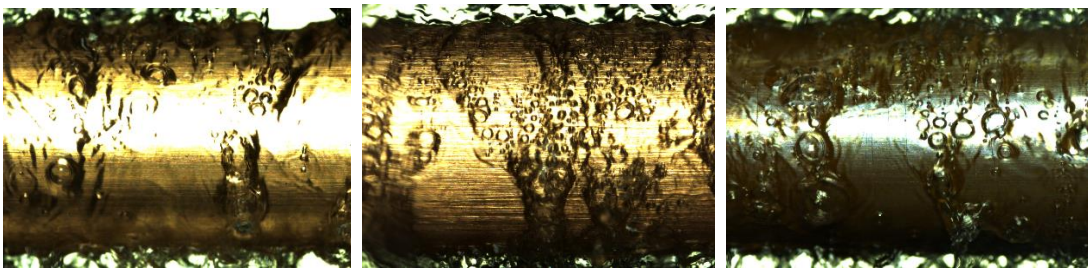

(a) Polished (b) Roughened (c) LbL

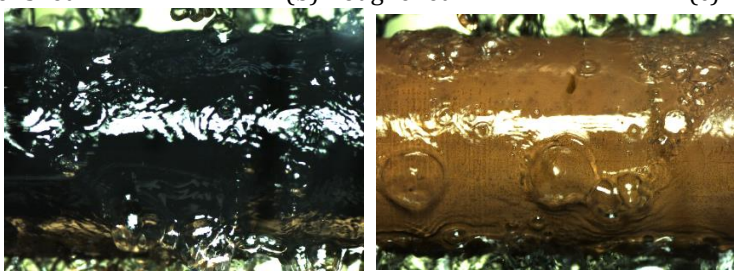

(d) CuO (e) nanoFLUX

Figure 13. Images of boiling surfaces at 20 kW/m^2 in R-245fa at 20 °C with a Γ_r of approximately 0.13 kg/m/s.

However, it is clear from the images that the roughened tube had the most bubbles. This agrees with the findings of the pool-boiling study where the roughened tube was found to have the most nucleation sites [40]. The 60 to 100% higher HTCs of the roughened tube compared with those of the polished tube seen in Figure 11 were thus likely due to increased nucleation site density, as the surfaces were otherwise structurally similar.

The LbL and CuO tubes had HTCs within 20% of the polished tube and it is not clear whether they had differing nucleation site densities based on Figure 13 compared with those of the polished tube. The nanoFLUX tube appeared to have a lower nucleation site density than for the roughened tube, as shown in Figure 13, despite having HTCs approximately 12% higher than for the roughened tube, with a similar trend seen in the pool-boiling results. This

suggested that the unique heat transfer mechanism of the nanoFLUX tube (and possibly the CuO tube) seen within our pool boiling study [40] was active under falling film conditions.

However, this evidence was not conclusive and an approach to measuring nucleation site density under falling film conditions would need to be developed to confirm this.

7.3. Falling film heat transfer enhancement

The falling film heat transfer enhancement ratios, K_{ff}, where the falling film HTCs at a Γ_r of approximately 0.13 kg/m/s were compared with the pool-boiling HTCs from our previous study [40] are shown in Figure 14 as a function of heat flux.

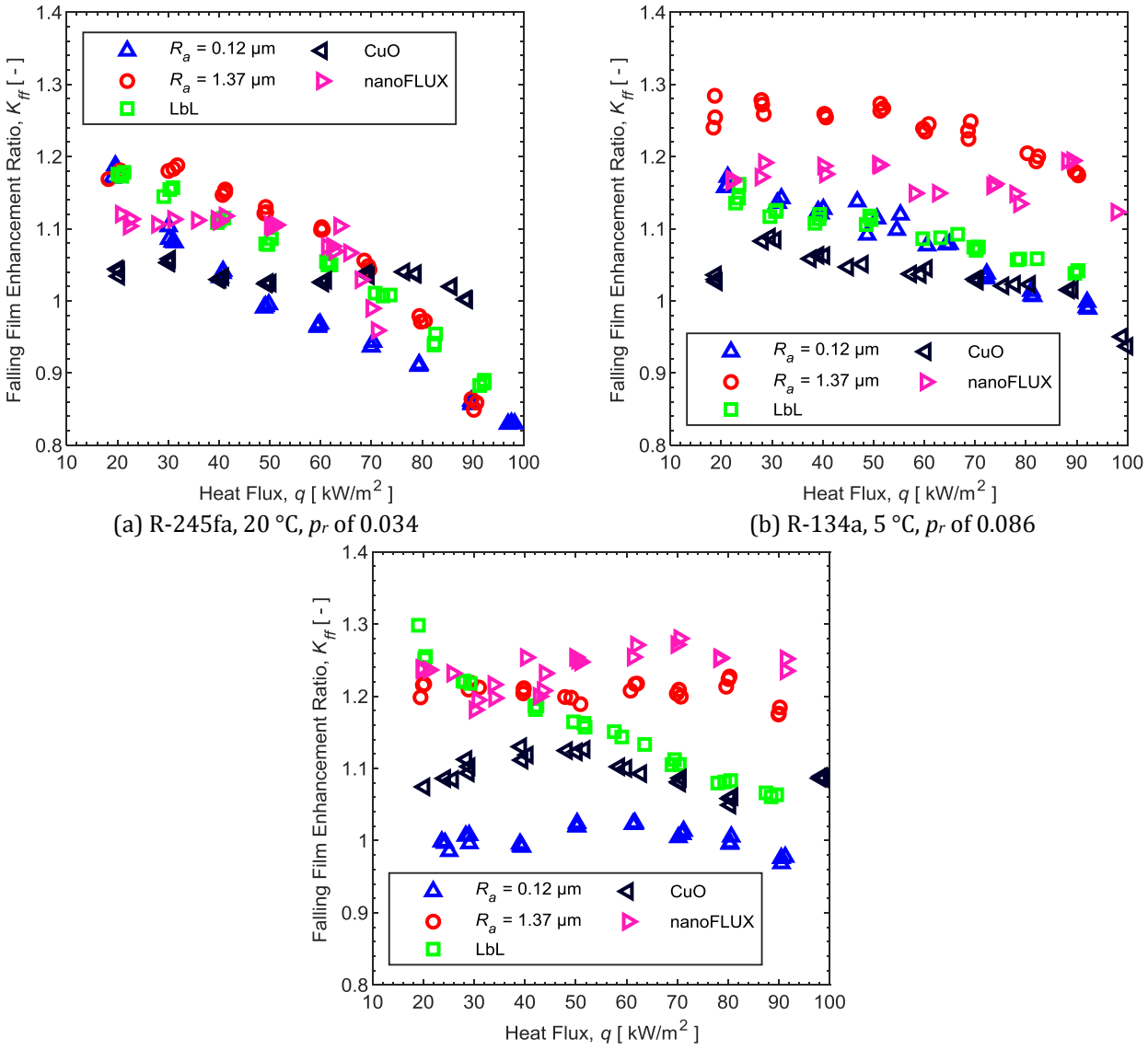

(a) R-245fa, 20 °C, p_r of 0.034

(b) R-134a, 5 °C, p_r of 0.086

(c) R-134a, 25 °C, p_r of 0.160

Figure 14. Falling film enhancement as a function of heat flux.

The polished tube had some of the lowest enhancement ratios, while the roughened tube had some of the highest enhancement ratios. This is consistent with the theory that falling film enhancement is driven by increased microlayer evaporation from trapped and sliding bubbles [8,64]. The greater nucleation site density of the roughened tube compared to the polished tube would allow it to have more sliding bubbles and thus a greater enhancement ratio. The LbL tube had an intermediate enhancement ratio throughout.

The nanoFLUX tube also had some of the highest falling film enhancement ratios measured, while the CuO surface had some of the lowest enhancement ratios. Considering that both the CuO and nanoFLUX surfaces had similar

nanostructures, it was likely that the difference in falling film enhancement ratios could also be attributed to differences in microstructure and the expected increased nucleation site density of the nanoFLUX tube, seen and measured in the pool-boiling results [40], which would result in a greater number of sliding bubbles.

It should be noted that the falling film enhancement of the nanostructured tubes was similar in magnitude to that of the plain tubes, while 3D micro-enhanced tubes showed falling film enhancement ratios as high as 2.5 [19]. Therefore, the unique heat transfer mechanisms of the nanostructured tubes appear not to be enhanced under falling film conditions and rather any enhancement appears to be through a similar mechanism to that of the plain tubes.

The falling film enhancement ratio of the polished, roughened and LbL surfaces all displayed a sensitivity to heat flux, particularly in R-245fa at 20 °C, while the nanoFLUX and CuO surface did not. This could be linked to dryout, because while our results showed that at similar film Reynolds number, R-134a at 25 °C had the worst dryout performance, at the same flow density of 0.13 kg/m/s, the worst dryout would occur in R-245fa at 20 °C because the film Reynolds number of R-245fa was approximately half that of R-134a due to R-245fa having over double the dynamic viscosity of R-134a at 20 °C.

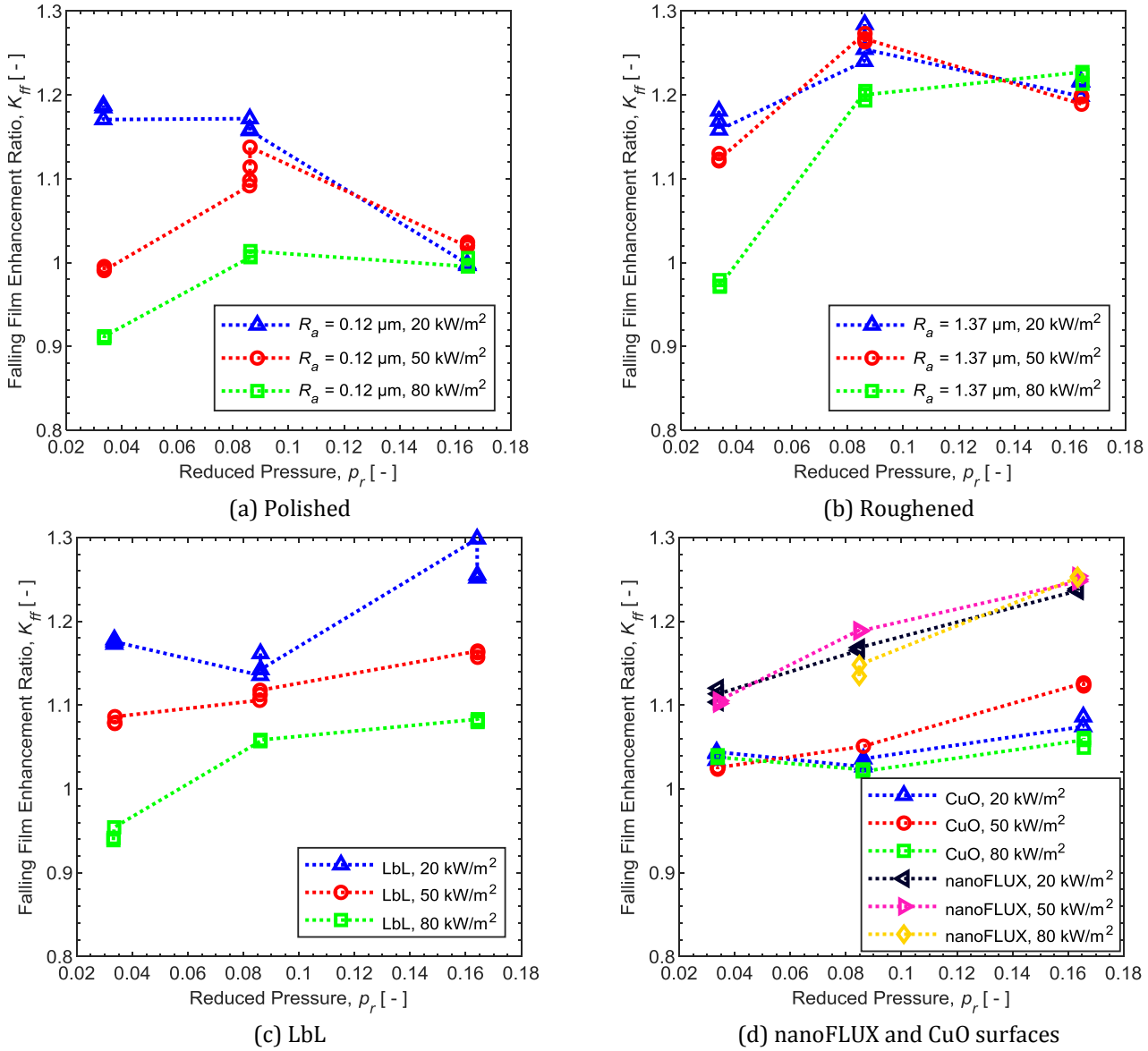

(a) Polished (b) Roughened

(c) LbL (d) nanoFLUX and CuO surfaces

Figure 15. K_{ff} as a function of p_r with Γ_r of approximately 0.13 kg/m/s.

The influence of reduced pressure on the falling film enhancement ratio is illustrated in Figure 15 at three heat fluxes of 20, 50 and 80 kW/m^2. The falling film enhancement ratio of the polished tube decreased as reduced pressure was increased at 20 kW/m^2, but increased at 80 kW/m^2. The roughened tube showed a relatively stable enhancement ratio at heat fluxes of 20 and 50 kW/m^2, but an increasing enhancement ratio at 80 kW/m^2.

The LbL, CuO and nanoFLUX tubes showed a clear increase in falling film enhancement ratios of approximately 10% as the reduced pressure was increased across the range of heat fluxes. This fits in with the already discussed theoretical framework, because increased reduced pressure leads to more activated nucleation sites and thus a greater number of sliding bubbles and increased microlayer evaporation than for pool boiling.

It is unclear why the polished tube had a reduction in enhancement ratio and the roughened tube enhancement ratio remained relatively constant as reduced pressure was increased at 20 kW/m^2. Dryout could be a factor, as the normalised HTCs in Figure 7 show that the polished and roughened tubes had a sensitive HTC plateau possibly caused by intermittent dryout. Therefore, at a Γ_r higher than those tested in this study, the HTCs of the polished and roughened tubes could increase and thus also increase the falling film enhancement ratio resulting in trends similar to those displayed by the CuO and nanoFLUX tubes, which had less of a dryout influenced plateau region.

8. Conclusions

The heat transfer coefficients (HTCs) on one polished, one roughened and three nanostructured horizontal tubes were measured during saturated falling film boiling of refrigerants R-245fa at 20 °C and R-134a at 5 °C and 25 °C. The refrigerant mass flow rate per unit length, Γ_r, on the outside of the tubes was varied from 0 kg/m/s to a maximum of approximately 0.13 kg/m/s. The three nanostructured tubes tested were: (i) an layer-by-layer (LbL) tube, created through the deposition of silica nanoparticles with a diameter of approximately 20 nm onto the surface of a CuO tube, (ii) a tube with copper oxide (CuO) nanostructures over its surface, created by using a chemical bath to oxidise the surface of the tube, and (iii) a commercial nanoFLUX-coated tube.

Both plain and nanostructured tubes displayed the characteristic plateau region with HTCs being relatively insensitive to reductions in Γ_r, followed by critical dryout where the HTCs collapsed as dry patches became predominant. The nanoFLUX tube, and the CuO tube to a lesser degree, produced a very insensitive plateau region as the Γ_r decreased, while the polished, roughened and LbL tubes all showed decreased HTCs within the plateau region up until the critical dryout limit. In some cases, an HTC hump was observed for the nanoFLUX tubes, where up to a 20% increase in the HTC occurred just prior to the critical dryout limit as the Γ_r was decreased. This was thought to be due to maintaining a very thin film of liquid that reduced the evaporative thermal resistance to a point where it could meaningfully contribute to the HTC.

Critical dryout occurred at higher film Reynolds numbers as the heat flux was increased for both plain and nanostructured tubes. The nanostructured CuO and nanoFLUX tubes had the lowest critical film Reynolds numbers at low heat fluxes (20 kW/m^2), but the highest critical film Reynolds numbers at higher heat fluxes (80 kW/m^2) due to the early onset of critical dryout or CHF at higher heat fluxes. The CuO and nanoFLUX tubes experienced early onset of CHF compared with the other tubes, with liquid separating and no longer wetting the surface of the tubes.

Evidence of wicking suggested that this was the mechanism that improved the dryout capabilities of the nanoFLUX and CuO tubes under lower heat flux conditions. However, increased heat fluxes possibly led to dryout over the CuO and nanoFLUX nanostructures resulting in operation in the Cassie-Baxter state and thus reduced wettability with subsequent critical dryout and critical heat flux occurring. The worst dryout performance was seen when boiling R-134 at 25 °C, followed by R-134a at 5 °C and then R245fa at 20 °C when compared on an equal film Reynolds number basis..

Nanostructured tubes achieved both higher and lower falling film boiling HTCs than those associated with the plain tubes over the heat flux range from 20 to 100 kW/m^2 at the maximum flow density of approximately 0.13 kg/m/s. The roughened tube had HTCs between 60% and 100% higher than the polished tube, the LbL tube had HTCs between 20% lower and 20% higher than the polished tube, the CuO tube had HTCs between 20% lower and 80% higher than the polished tube, and the nanoFLUX tube had between 40 to 200% higher HTCs than the polished tube. Both plain and nanostructured tubes had HTCs that increased as the heat flux or reduced pressure were increased. The CuO and nanoFLUX tubes showed higher sensitivities to changes in the heat flux and reduced pressure than the other tubes.

The falling film heat transfer enhancement ratios of the nanostructured tubes tested in this study were of a similar order of magnitude to those of the plain tubes. The enhancement ratios of the LbL, CuO and nanoFLUX nanostructured tubes increased as the reduced pressure was increased, thought to be caused by increased bubble nucleation at higher reduced pressures resulting in greater microfilm evaporation from sliding bubbles. The falling film heat transfer enhancement ratios of the roughened and nanoFLUX tubes were higher than those of the polished and CuO tubes respectively, likely as a result of a greater number of active nucleation sites on the roughened and nanoFLUX tubes. The polished and roughened tube falling film heat transfer enhancement ratios did not increase monotonically as the reduced pressure increased, possibly as a result of dryout considerations.

Credit authorship contribution statement

Bradley D. Bock: Conceptualisation, methodology, validation, formal analysis, investigation, data curation, visualisation, writing – original draft, project administration. **Matteo Bucci:** Conceptualisation, funding acquisition, resources, supervision, writing – review and editing. **Christos N. Markides:** Conceptualisation, funding acquisition, writing – review and editing. **John R. Thome:** Conceptualisation, methodology, funding acquisition, resources, supervision, writing – review and editing. **Josua P. Meyer:** Conceptualisation, methodology, funding acquisition, resources, supervision, writing – review and editing.

Declaration of competing interest

The authors declare that there are no conflicts of interest.

Acknowledgements

This work was supported by the MIT International Science and Technology Initiatives (MISTI) programme under an MIT-Africa-Imperial College London seed fund grant, by the UK Department for International Development (DFID) through the Royal Society-DFID Africa Capacity Building Initiative and by the European Union's Horizon 2020 Research and Innovation Programme within the ThermaSMART network under the Marie Sklodowska-Curie Grant Agreement No. 778104. The authors would also like to acknowledge Dr Victor Voulgaropoulos for assistance with the MIT-Africa-Imperial College London seed fund grant, Dr Alexander Reip and Tim Bullen of Oxford nanoSystems and Chi Wang and Dr Bren Phillips at MIT for assistance with the coatings, as well as Dr Dorette Kritzinger and Professor Jackie Nel at the University of Pretoria for assistance with the surface characterisation.

References

[1] S. Kalliadasis, C. Ruyer-Quil, B. Scheid, and M. G. Velarde, *Falling liquid films*. Springer Science & Business Media, 2011.

[2] F. Denner, A. Charogiannis, M. Pradas, C. N. Markides, B. G. M. van Wachem, and S. Kalliadasis, "Solitary waves on falling liquid films in the inertia-dominated regime," *Journal of Fluid Mechanics,* vol. 837, pp. 491-519, 2018.

[3] K. Moran, J. Inumaru, and M. Kawaji, "Instantaneous hydrodynamics of a laminar wavy liquid film," *International Journal of Multiphase Flow,* vol. 28, no. 5, pp. 731-755, 2002.

[4] A. Charogiannis and C. N. Markides, "Spatiotemporally resolved heat transfer measurements in falling liquid-films by simultaneous application of planar laser-induced fluorescence (PLIF), particle tracking velocimetry (PTV) and infrared (IR) thermography," *Experimental Thermal and Fluid Science,* vol. 107, pp. 169-191, 2019.

[5] S. V. Alekseenko, V. E. Nakoryakov, and B. G. Pokusaev, "Wave effect on the transfer processes in liquid films," *Chemical Engineering Communications,* vol. 141-142, no. 1, pp. 359-385, 1996.

[6] E. A. Chinnov, E. N. Shatskii, and O. A. Kabov, "Evolution of the temperature field at the three-dimensional wave front in a heated liquid film," *High Temperature,* vol. 50, no. 1, pp. 98-105, 2012.

[7] V. I. Zhukov and A. N. Pavlenko, "Heat transfer and critical phenomena during evaporation and boiling in a thin horizontal liquid layer at low pressures," *International Journal of Heat and Mass Transfer,* vol. 117, pp. 978-990, 2018.

[8] R. Mesler, "A mechanism supported by extensive experimental evidence to explain high heat fluxes observed during nucleate boiling," *AIChE Journal,* vol. 22, no. 2, pp. 246-252, 1976.

[9] M. Cerza and V. Sernas, "Nucleate boiling in thermally developing and fully developed laminar falling water films," *Journal of Heat Transfer,* vol. 110, no. 1, pp. 221-228, 1988.

[10] A. Surtaev and A. Pavlenko, "Observation of boiling heat transfer and crisis phenomena in falling water film at transient heating," *International Journal of Heat and Mass Transfer,* vol. 74, pp. 342-352, 2014.

[11] I. A. Mudawwar, T. A. Incropera, and F. P. Incropera, "Boiling heat transfer and critical heat flux in liquid films falling on vertically-mounted heat sources," *International Journal of Heat and Mass Transfer,* vol. 30, no. 10, pp. 2083-2095, 1987.

[12] G. Ribatski and A. M. Jacobi, "Falling-film evaporation on horizontal tubes - A critical review," *International Journal of Refrigeration,* vol. 28, no. 5, pp. 635-653, 2005.

[13] J. R. Thome, "Engineering data book 3," *Wolverine Tube Inc,* 2004.

[14] J. F. Roques and J. R. Thome, "Falling films on arrays of horizontal tubes with R134a, part 1: Boiling heat transfer results for four types of tubes," *Heat Transfer Engineering,* vol. 28, no. 5, pp. 398-414, 2007.

[15] P.-H. Jin, Z. Zhang, I. Mostafa, C.-Y. Zhao, W.-T. Ji, and W.-Q. Tao, "Heat transfer correlations of refrigerant falling film evaporation on a single horizontal smooth tube," *International Journal of Heat and Mass Transfer,* vol. 133, pp. 96-106, 2019.
[16] C.-Y. Zhao, P.-H. Jin, W.-T. Ji, Y.-L. He, and W.-Q. Tao, "Experimental investigations of R134a and R123 falling film evaporation on enhanced horizontal tubes," *International Journal of Refrigeration,* vol. 75, pp. 190-203, 2017.
[17] P.-H. Jin, C.-Y. Zhao, W.-T. Ji, and W.-Q. Tao, "Experimental investigation of R410A and R32 falling film evaporation on horizontal enhanced tubes," *Applied Thermal Engineering,* vol. 137, pp. 739-748, 2018.
[18] P.-H. Jin, Z. Zhang, I. Mostafa, C.-Y. Zhao, W.-T. Ji, and W.-Q. Tao, "Experimental study of falling film evaporation in tube bundles of doubly-enhanced, horizontal tubes," *Applied Thermal Engineering,* vol. 170, p. 115006, 2020.
[19] M. Christians and J. R. Thome, "Falling film evaporation on enhanced tubes, part 1: Experimental results for pool boiling, onset-of-dryout and falling film evaporation," *International Journal of Refrigeration,* vol. 35, no. 2, pp. 300-312, 2012.
[20] D. Jige, H. Miyata, and N. Inoue, "Falling film evaporation of R1234ze(E) and R245fa on a horizontal smooth tube," *Experimental Thermal and Fluid Science,* vol. 105, pp. 58-66, 2019.
[21] S. A. Moeykens and M. B. Pate, "Spray evaporation heat transfer of R134a on plain tubes," in *American Society of Heating, Refrigerating, and Air Conditioning Engineers (ASHRAE) annual meeting*, Orlando, FL (United States), 1994, vol. 100, pp. 173-184: American Society of Heating, Refrigerating and Air-Conditioning Engineers, Inc., .
[22] D. E. Kim, D. I. Yu, D. W. Jerng, M. H. Kim, and H. S. Ahn, "Review of boiling heat transfer enhancement on micro/nanostructured surfaces," *Experimental Thermal and Fluid Science,* vol. 66, pp. 173-196, 2015.
[23] X. Li, I. Cole, and J. Tu, "A review of nucleate boiling on nanoengineered surfaces: The nanostructures, phenomena and mechanisms," *International Journal of Heat and Mass Transfer,* vol. 141, pp. 20-33, 2019.
[24] K.-H. Chu, Y. S. Joung, R. Enright, C. R. Buie, and E. N. Wang, "Hierarchically structured surfaces for boiling critical heat flux enhancement," *Applied Physics Letters,* vol. 102, no. 15, p. 151602, 2013.
[25] T. Ubara, H. Asano, and K. Sugimoto, "Heat transfer enhancement of falling film evaporation on a horizontal tube by thermal spray coating," *Applied Sciences,* vol. 10, no. 5, p. 1632, 2020.
[26] Y. Zheng, X. Ma, Y. Li, R. Jiang, K. Wang, Z. Lan, and Q. Liang, "Experimental study of falling film evaporation heat transfer on superhydrophilic horizontal-tubes at low spray density," *Applied Thermal Engineering,* vol. 111, pp. 1548-1556, 2017.
[27] B. Köroğlu, K. S. Lee, and C. Park, "Nano/micro-scale surface modifications using copper oxidation for enhancement of surface wetting and falling-film heat transfer," *International Journal of Heat and Mass Transfer,* vol. 62, pp. 794-804, 2013.
[28] S. Lee, B. Köroğlu, and C. Park, "Experimental investigation of capillary-assisted solution wetting and heat transfer using a micro-scale, porous-layer coating on horizontal-tube, falling-film heat exchanger," *International Journal of Refrigeration,* vol. 35, no. 4, pp. 1176-1187, 2012.
[29] C.-Y. Zhao, W.-T. Ji, P.-H. Jin, and W.-Q. Tao, "Heat transfer correlation of the falling film evaporation on a single horizontal smooth tube," *Applied Thermal Engineering,* vol. 103, no. Supplement C, pp. 177-186, 2016.
[30] B. D. Bock, J. P. Meyer, and J. R. Thome, "Falling film boiling and pool boiling on plain circular tubes: Influence of surface roughness, surface material and saturation temperature on heat transfer and dryout," *Experimental Thermal and Fluid Science,* vol. 109, p. 109870, 2019.
[31] J. Barber, D. Brutin, and L. Tadrist, "A review on boiling heat transfer enhancement with nanofluids," *Nanoscale Research Letters,* vol. 6, no. 1, p. 280, 2011.
[32] M. Shojaeian and A. Koşar, "Pool boiling and flow boiling on micro- and nanostructured surfaces," *Experimental Thermal and Fluid Science,* vol. 63, pp. 45-73, 2015.
[33] C. S. Sujith Kumar, G. Udaya Kumar, M. R. Mata Arenales, C.-C. Hsu, S. Suresh, and P.-H. Chen, "Elucidating the mechanisms behind the boiling heat transfer enhancement using nano-structured surface coatings," *Applied Thermal Engineering,* vol. 137, pp. 868-891, 2018.
[34] C. G. Jothi Prakash and R. Prasanth, "Enhanced boiling heat transfer by nano structured surfaces and nanofluids," *Renewable and Sustainable Energy Reviews,* vol. 82, pp. 4028-4043, 2018.
[35] Y. Im, Y. Joshi, C. Dietz, and S. S. Lee, "Enhanced boiling of a dielectric liquid on copper nanowire surfaces," *International Journal of Micro-Nano Scale Transport,* vol. 1, no. 1, pp. 79-96, 2010.
[36] G. Udaya Kumar, S. Suresh, M. R. Thansekhar, and P. Dinesh Babu, "Effect of diameter of metal nanowires on pool boiling heat transfer with FC-72," *Applied Surface Science,* vol. 423, pp. 509-520, 2017.
[37] W. Wu, H. Bostanci, L. C. Chow, Y. Hong, M. Su, and J. P. Kizito, "Nucleate boiling heat transfer enhancement for water and FC-72 on titanium oxide and silicon oxide surfaces," *International Journal of Heat and Mass Transfer,* vol. 53, no. 9, pp. 1773-1777, 2010.

[38] B. S. Kim, G. Choi, D. I. Shim, K. M. Kim, and H. H. Cho, "Surface roughening for hemi-wicking and its impact on convective boiling heat transfer," *International Journal of Heat and Mass Transfer,* vol. 102, pp. 1100-1107, 2016.
[39] V. Trisaksri and S. Wongwises, "Nucleate pool boiling heat transfer of TiO2–R141b nanofluids," *International Journal of Heat and Mass Transfer,* vol. 52, no. 5, pp. 1582-1588, 2009.
[40] B. D. Bock, M. Bucci, C. N. Markides, J. R. Thome, and J. P. Meyer, "Pool boiling of refrigerants over nanostructured and roughened tubes," *International Journal of Heat and Mass Transfer,* vol. 162, p. 120387, 2020.
[41] M. Zimmermann, M. Heinz, A. Sielaff, T. Gambaryan-Roisman, and P. Stephan, "Influence of system pressure on pool boiling regimes on a microstructured surface compared to a smooth surface," *Experimental Heat Transfer,* pp. 1-17, 2019.
[42] S. Shin, G. Choi, B. S. Kim, and H. H. Cho, "Flow boiling heat transfer on nanowire-coated surfaces with highly wetting liquid," *Energy,* vol. 76, pp. 428-435, 2014.
[43] T. Ueda, M. Inoue, and S. Nagatome, "Critical heat flux and droplet entrainment rate in boiling of falling liquid films," *International Journal of Heat and Mass Transfer,* vol. 24, no. 7, pp. 1257-1266, 1981.
[44] R. P. Baines, M. A. El Masri, and W. M. Rohsenow, "Critical heat flux in flowing liquid films," *International Journal of Heat and Mass Transfer,* vol. 27, no. 9, pp. 1623-1629, 1984.
[45] T. A. Grimley, I. Mudawwar, and F. P. Incropera, "CHF enhancement in flowing fluorocarbon liquid films using structured surfaces and flow deflectors," *International Journal of Heat and Mass Transfer,* vol. 31, no. 1, pp. 55-65, 1988.
[46] G. Ribatski and J. R. Thome, "A visual study of R134a falling film evaporation on enhanced and plain tubes," presented at the 5th International Symposium on Multiphase Flow, Heat Mass Transfer and Energy Conversion, Xi'an, China, 3-6 July, 2005, 2005. Available: http://infoscience.epfl.ch/record/52919
[47] F. Ç. Cebeci, Z. Wu, L. Zhai, R. E. Cohen, and M. F. Rubner, "Nanoporosity-driven superhydrophilicity: A means to create multifunctional antifogging coatings," *Langmuir,* vol. 22, no. 6, pp. 2856-2862, 2006.
[48] E. Forrest, E. Williamson, J. Buongiorno, L.-W. Hu, M. Rubner, and R. Cohen, "Augmentation of nucleate boiling heat transfer and critical heat flux using nanoparticle thin-film coatings," *International Journal of Heat and Mass Transfer,* vol. 53, no. 1, pp. 58-67, 2010.
[49] Y. Nam and Y. S. Ju, "A comparative study of the morphology and wetting characteristics of micro/nanostructured Cu surfaces for phase change heat transfer applications," *Journal of Adhesion Science and Technology,* vol. 27, no. 20, pp. 2163-2176, 2013.
[50] H. O'Hanley, C. Coyle, J. Buongiorno, T. McKrell, L.-W. Hu, M. Rubner, and R. Cohen, "Separate effects of surface roughness, wettability, and porosity on the boiling critical heat flux," *Applied Physics Letters,* vol. 103, no. 2, p. 024102, 2013.
[51] M. Tetreault-Friend, R. Azizian, M. Bucci, T. McKrell, J. Buongiorno, M. Rubner, and R. Cohen, "Critical heat flux maxima resulting from the controlled morphology of nanoporous hydrophilic surface layers," *Applied Physics Letters,* vol. 108, no. 24, p. 243102, 2016.
[52] A. F. Stalder, T. Melchior, M. Müller, D. Sage, T. Blu, and M. Unser, "Low-bond axisymmetric drop shape analysis for surface tension and contact angle measurements of sessile drops," *Colloids and Surfaces A: Physicochemical and Engineering Aspects,* vol. 364, no. 1, pp. 72-81, 2010.
[53] W. S. Rasband, "ImageJ," ed: Bethesda, MD, 1997.
[54] J. Drelich, E. Chibowski, D. D. Meng, and K. Terpilowski, "Hydrophilic and superhydrophilic surfaces and materials," *Soft Matter,* 10.1039/C1SM05849E vol. 7, no. 21, pp. 9804-9828, 2011.
[55] X. Yan, Z. Huang, S. Sett, J. Oh, H. Cha, L. Li, L. Feng, Y. Wu, C. Zhao, D. Orejon, F. Chen, and N. Miljkovic, "Atmosphere-mediated superhydrophobicity of rationally designed micro/nanostructured surfaces," *ACS Nano,* vol. 13, no. 4, pp. 4160-4173, 2019.
[56] M. Christians, "Heat transfer and visualization of falling film evaporation on a tube bundle," Ph.D., École Polytechnique Fédérale de Lausanne, Lausanne, Switzerland, 2010.
[57] E. W. Lemmon, M. L. Huber, and M. O. McLinden, "NIST reference fluid thermodynamic and transport properties—REFPROP," *NIST Standard Reference Database,* vol. 23, p. v7, 2002.
[58] E. Van Rooyen, M. Christians, and J. R. Thome, "Modified Wilson plots for enhanced heat transfer experiments: Current status and future perspectives," *Heat Transfer Engineering,* vol. 33, no. 4-5, pp. 342-355, 2012.
[59] V. Gnielinski, "New equations for heat and mass-transfer in turbulent pipe and channel flow," *International Chemical Engineering,* vol. 16, no. 2, pp. 359-368, 1976.
[60] P. F. Dunn, *Measurement and data analysis for engineering and science*, 2nd ed. CRC press, 2010.
[61] I. BIPM, I. IFCC, I. ISO, and O. IUPAP, "Evaluation of measurement data—guide to the expression of uncertainty in measurement, JCGM 100: 2008 GUM 1995 with minor corrections.," *Joint Committee for Guides in Metrology,* 2008.

[62] M.-C. Chyu and A. Bergles, "Horizontal-tube falling-film evaporation with structured surfaces," *Journal of Heat Transfer,* vol. 111, no. 2, pp. 518-524, 1989.
[63] M. C. Chyu, J. Zheng, and Z. Ayub, "Bundle effect of ammonia/lubricant mixture boiling on a horizontal bundle with enhanced tubing and inlet quality," *International Journal of Refrigeration,* vol. 32, no. 8, pp. 1876-1885, 2009.
[64] M. Cerza and V. Sernas, "A bubble growth model for nucleate boiling in thin, falling, superheated, laminar, water films," *International Journal of Heat and Mass Transfer,* vol. 28, no. 7, pp. 1307-1316, 1985.

Highlights

- Nanostructured and plain tubes tested under falling film boiling conditions
- Heat transfer coefficients measured in refrigerants R-134a and R-245fa
- Critical dryout and critical heat flux identified
- Falling film heat transfer coefficients compared to those of pool boiling

View publication stats